JOURNAL OF GEOPHYSICAL RESEARCH, VOL. 108, NO. D9, 4291, doi:10.1029/2002JD002912, 2003

Tropospheric ozone at tropical and middle latitudes derived from TOMS/MLS residual: Comparison with a global model

S. Chandra
NASA Goddard Space Flight Center, Greenbelt, Maryland, USA

J. R. Ziemke
Goddard Earth Sciences and Technology Center, University of Maryland, Baltimore County, Baltimore, Maryland, USA

R. V. Martin[1]
Department of Earth and Planetary Sciences Division of Engineering and Applied Sciences, Harvard University, Cambridge, Massachusetts, USA

Received 5 September 2002; revised 11 December 2002; accepted 8 January 2003; published 13 May 2003.

[1] The tropospheric ozone residual method is used to derive zonal maps of tropospheric column ozone using concurrent measurements of total column ozone from Nimbus 7 and Earth Probe (EP) Total Ozone Mapping Spectrometer (TOMS) and stratospheric column ozone from the Microwave Limb Sounder (MLS) instrument on the Upper Atmosphere Research Satellite (UARS). Our study shows that the zonal variability in TOMS total column ozone at tropical and subtropical latitudes is mostly of tropospheric origin. The seasonal and zonal variability in tropospheric column ozone (TCO), derived from the TOMS/MLS residual, is consistent with that derived from the convective cloud differential method and ozonesonde measurements in regions where these data overlap. A comparison of TCO derived from the TOMS/MLS residual and a global three-dimensional model of tropospheric chemistry (GEOS-CHEM) for 1996–1997 shows good agreement in the tropics south of the equator. Both the model and observations show similar zonal and seasonal characteristics including an enhancement of TCO in the Indonesian region associated with the 1997 El Niño. Both show the decline of the wave-1 pattern from the tropics to the extratropics as lightning activity and the Walker circulation decline. Both show enhanced ozone in the downwelling branches of the Hadley Circulation near $\pm 30^{o}$. Model and observational differences increase with latitude during winter and spring. *INDEX TERMS:* 0365 Atmospheric Composition and Structure: Troposphere—composition and chemistry; 0368 Atmospheric Composition and Structure: Troposphere—constituent transport and chemistry; 3309 Meteorology and Atmospheric Dynamics: Climatology (1620); 3319 Meteorology and Atmospheric Dynamics: General circulation; 3360 Meteorology and Atmospheric Dynamics: Remote sensing; *KEYWORDS:* biomass burning, tropospheric ozone, stratospheric ozone, El Niño, global circulation model, tropopause

Citation: Chandra, S., J. R. Ziemke, and R. V. Martin, Tropospheric ozone at tropical and middle latitudes derived from TOMS/MLS residual: Comparison with a global model, *J. Geophys. Res.*, *108*(D9), 4291, doi:10.1029/2002JD002912, 2003.

1. Introduction

[2] Many of the current techniques for deriving tropospheric ozone from satellite measurements are limited to tropical latitudes [*Jiang and Yung*, 1996; *Kim and Newchurch*, 1996; *Hudson and Thompson*, 1998; *Ziemke et al.*, 1998, 2001; *Thompson and Hudson*, 1999; *Kim et al.*, 2001]. They are based on the tropospheric ozone residual (TOR) method, which derives tropospheric column ozone (TCO) by subtracting concurrent measurements of stratospheric column ozone (SCO) from total column ozone measured by the TOMS instrument [*Fishman and Larsen*, 1987]. J. Fishman and his colleagues [*Fishman and Larsen*, 1987; *Fishman et al.*, 1990], who first introduced the TOR concept, used concurrent total column ozone measurements from TOMS instrument and SCO from SAGE (Stratospheric Aerosol and Gas Experiment) instrument to derive TCO. SAGE, being an occultation measuring instrument could not be used for anything other than climatological studies. *Fishman and Balok* [1999] have attempted to account for this shortcoming by replacing SAGE profiles with profiles derived from the solar backscatter ultraviolet (SBUV) measurements. Unlike SAGE, the SBUV profiles provide daily global maps of SCO with the caveat that SBUV has a limited profile information in the lowest three Umkehr layers from the ground to 63 hPa. Assuming that

[1]Now at Harvard-Smithsonian Center for Astrophysics, Cambridge, Mass, 02138, USA.

0148-0227/03/2002JD002912

the integrated column ozone amount from ground to 63 hPa are correctly measured by SBUV, *Fishman and Balok* [1999] applied a normalization correction to SBUV profile measurements using ozonesonde climatology.

[3] The CCD technique [*Ziemke et al.*, 1998], which is another version of TOR methodology, takes advantage of the fact that for UV measuring instruments, such as TOMS, optically thick clouds obscure ozone below. Therefore, one can make a fairly accurate estimate of SCO using high reflecting convective cloud scenes ($R > 0.9$) near the tropopause in the tropical Pacific region. The CCD method further assumes that the SCO is zonally invariant within 15°N and 15°S. TCO is calculated using the total columns determined from the low reflecting scenes ($R < 0.2$) and the stratospheric columns using high reflecting scenes ($R > 0.9$).

[4] *Chandra et al.* [2002] and *Martin et al.* [2002] have shown that most of the observed characteristics of ozone time series, derived from the CCD technique, are well characterized by the GEOS-CHEM 3-D tropospheric chemistry and transport model. These characteristics include seasonal variations and anomalously large increases in TCO in the Indonesian region during September–December 1997, following large scale forest fires and Savanna burning [*Chandra et al.*, 1998; *Thompson et al.*, 2001]. El Niño induced changes in tropospheric ozone, derived from the CCD technique, were also analyzed by *Sudo and Takahashi* [2001], using a 3-D photochemical model developed at the Center for Climate Research, University of Tokyo, Japan [*Sudo et al.*, 2002]. They were able to simulate most of the observed changes in tropospheric ozone related to 1997 El Niño and concluded, as did *Chandra et al.* [1998, 2002], that both the biomass burning and the changes in meteorological conditions (e.g., low convective activity, sparse precipitation, dry air condition, enhanced transport from stratosphere) contributed almost equally to the observed enhancement in tropospheric ozone.

[5] The comparison of the model and CCD tropospheric ozone has not been very satisfactory north of the equator in the African region. During the 1996–1997 period, observed TCO tends to have a broad peak in late fall (September–November) and a deep minimum in early spring (February–March) similar to TCO seasonality south of the equator in the Atlantic region. The model phase is just the opposite and seems to be in accord with the burning season of northern Africa. *Martin et al.* [2002] have studied these differences in detail and have noted similar differences between model and CCD TCO over Southeast Asia. In both these regions the model seasonality in TCO tends to be in general agreement with ozone seasonality inferred from the Measurement of Ozone and Water Vapor by Airbus In-Service Aircraft (MOZAIC) science program [*Marenco et al.*, 1998].

[6] The purpose of this paper is to develop a methodology of deriving TCO, which will compliment the CCD method in the tropics but which could be used to extend our measurement capability to higher latitudes for comparison with global models. This methodology is based on the TOR principle that uses concurrent total column ozone measurements from the TOMS instrument and SCO measurements from the MLS (Microwave Limb Sounding) instrument on UARS (Upper Atmosphere Research Satellite) as discussed by *Ziemke et al.* [1998]. We will show that concurrent measurements of ozone from these instruments can be used to generate global maps of column ozone from ground to 100 hPa and TCO maps over latitudes from 30°N to 30°S. These maps in conjunction with ozonesonde measurements are analyzed to gain further insight into the differences of modeled and observed ozone in the troposphere.

[7] The following sections begin with the description of the MLS and TOMS data followed by cross calibration of TOMS and MLS instruments (sections 2 and 3), validation with ozone sonde (section 4), and characterization of high-resolution global maps of ozone column from ground to 100 hPa (section 5). Sections 6 and 7 discuss the methodology for correcting for excess ozone between tropopause and 100 hPa and the error in deriving TCO. Section 8 compares the zonal characteristics of TCO derived from the TOMS/MLS and CCD methods and discusses the zonal characteristics of SCO derived from MLS. Finally, section 9 compares the TCO derived from TOMS/MLS residual with a global 3-D model of tropospheric chemistry (GEOS-CHEM) and section 10summarizes the main results of this paper.

2. MLS Version 5 Data, Nimbus 7, and EP TOMS Version 7 Data

[8] The total column ozone needed to derive TCO from TOMS/MLS residual is available in $1° \times 1°$ grid size on a daily basis from January 1979 to April 1993 from Nimbus 7 TOMS and from July 1996 to the present time from EP TOMS (http://toms.gsfc.nasa.gov). The MLS ozone measurements cover only a part of this time interval beginning from September 1991 to the middle of 1998 (see MLS web page http://mls.jpl.nasa.gov for details). As a result the MLS and TOMS measurements overlap only for about 20 months (September 1991–April 1993) during the Nimbus 7 TOMS lifetime and about two years (August 1996–mid 1998) during the EP TOMS time period. The frequency of measurements of the MLS instrument also changes over the course of the MLS life cycle from almost daily measurements during the Nimbus 7 period to only a few days (5–10 days per month on average) during the EP TOMS period. Their latitudinal coverage also differs. Both Nimbus 7 and EP TOMS were placed in sun synchronous orbits, which provided almost pole-to-pole measurements. The MLS measurements cover a latitude range from 34° to 80°, which alternate from north to south about every 36 days on average. This is because of the 57° inclination of the UARS orbit and planned rotation of the satellite through 180° in yaw about every 36 days [*Reber*, 1993]. The MLS instrument measures ozone profiles at both ascending and descending orbital paths. For MLS the optical length for the detected limb emission is around 400 km [*Froidevaux et al.*, 1996]. Level 3AT MLS measurements as noted by *Froidevaux et al.* [1996] have typically 1318 or 1319 profile measurements per day over the globe. These profiles provide a mean horizontal "footprint" measurement of around 1500 km (zonal) by 200 km (meridional). The calculated SCO from MLS profiles was binned spatially to a $5° \times 5°$ grid following a subjective 2-D (latitude-longitude) linear interpolation. In calculating TOR, we have also degraded TOMS spatial resolution from $1° \times 1°$ grid size to $5° \times 5°$ grid size. The only exceptions are the high-resolution maps (Figures 5a and 5b). They are based on high-resolution ($1° \times 1°$) maps of TOMS total column

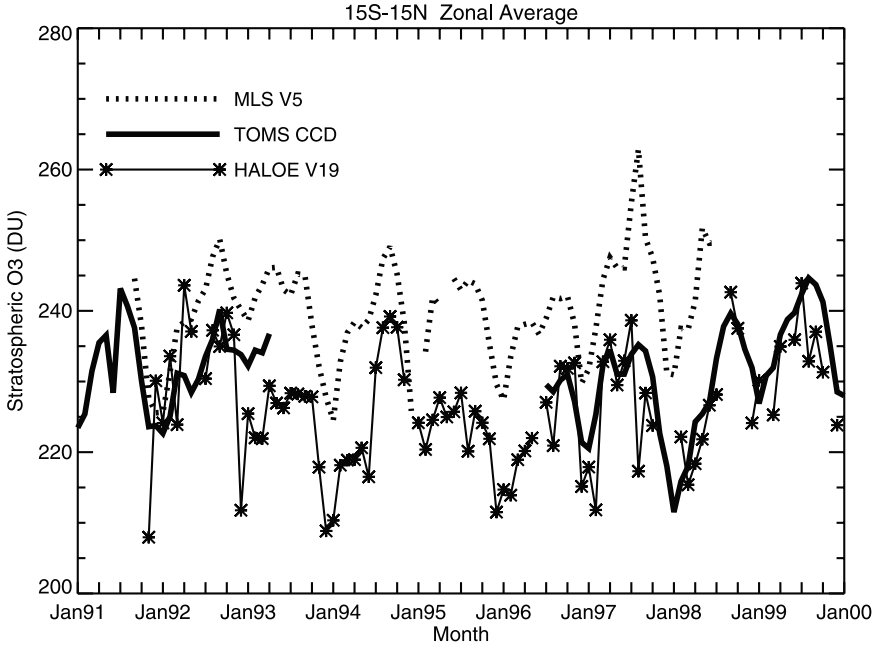

Figure 1. Stratospheric column ozone time series (in Dobson units) averaged over area in the tropics between latitudes 15°S and 15°N for MLS version 5 (dotted), TOMS CCD (solid), and HALOE version 19 (stars). Time coverage plotted: Years 1991 through 1999.

ozone using further interpolation of stratospheric column amounts down to a smaller scale of $1° \times 1°$.

[9] Stratospheric measurements from MLS, used by *Ziemke et al.* [1998], were based on the version 4 algorithm, which retrieved ozone profiles down to 46 hPa and not to tropopause level. To account for the SCO burden between 46 hPa and the tropopause, Halogen Occultation Experiment (HALOE) ozone data [*Brühl et al.*, 1996] were assimilated with MLS to determine daily maps of SCO. MLS version 5 (v5) algorithm retrieves ozone profiles down to 100 hPa [*Livesey et al.*, 2003]. Since this is close to tropopause level at tropical and subtropical latitudes, it eliminates the need to use HALOE data for assimilation. A detailed account of the v5 MLS ozone profile used in this paper is given by *Livesey et al.* [2003]. These profiles are based on the data from the 205 GHz radiometer channel. The recommended vertical range for use of v5 205 GHz ozone extends from 100 to 0.2 hPa. Though MLS v5 profiles show much better agreement with ozonesonde and SAGE II profiles compared to v4, significant differences between these measurements remain particularly in the lower stratosphere. The v5 MLS ozone values at 68 and 100 hPa appear to be systematically larger than ozonesonde by 10–15 %. The MLS/SAGE II (version 6.1 SAGE) comparisons also indicate higher values for MLS. However, MLS/Sonde differences are relatively larger than MLS/SAGE. It is, therefore, apparent that before TCO can be determined from differencing TOMS total column ozone and MLS SCO, the two instruments need inter-instrument calibration of their column ozone measurements.

3. TOMS/MLS Cross Calibration

[10] The simplest way to achieve the TOMS/MLS cross calibration is to adjust the MLS SCO to SCO derived from the TOMS CCD using a linear regression method. Figure 1 shows monthly mean time series of stratospheric column ozone from 100 hPa to the top of the atmosphere using three independent measurements from MLS, HALOE and TOMS CCD. These time series were derived using all available measurements from 1991 to 2000 over the latitude band 15°S to 15°N. They represent temporal characteristics of SCO in the tropics where the tropopause is close to 100 hPa. As an occultation measurement, HALOE has sparse coverage in the tropics (around 2 measurements per month). Yet the HALOE time series is remarkably similar to CCD both with respect to its temporal characteristics and absolute values. The MLS time series shows similar temporal characteristics, but with a significant bias with respect to the two time series. The absolute values of SCO inferred from the MLS time series tend to be higher by 5–10 Dobson units (DU) during the Nimbus 7 time period (1991–1993) and by 15–20 DU during the Earth Probe TOMS period (1996–1998). The increase in MLS bias with respect to HALOE or TOMS during the latter period may be related to changes in the retrieval algorithm of v5 MLS with respect to the earlier period. The 63 GHz radiometer channel, which was used to retrieve temperature and pressure profiles, was switched off after June 15, 1997 to lower the power requirement of the MLS instrument. As a result, the retrieval algorithm after this period used the tangent pressure deduced from the 205-GHz channel instead of 63 GHz channel used previously. In addition, the daily coverage of the MLS data decreased significantly after 1995 from almost every day before 1995 to about 5–10 days per month on average during the 1996–1998 period.

[11] Figure 2 shows the adjusted MLS time series using the linear regression analysis of CCD and unadjusted MLS time series. The agreement between the CCD and adjusted MLS time series is remarkably good with a difference of at

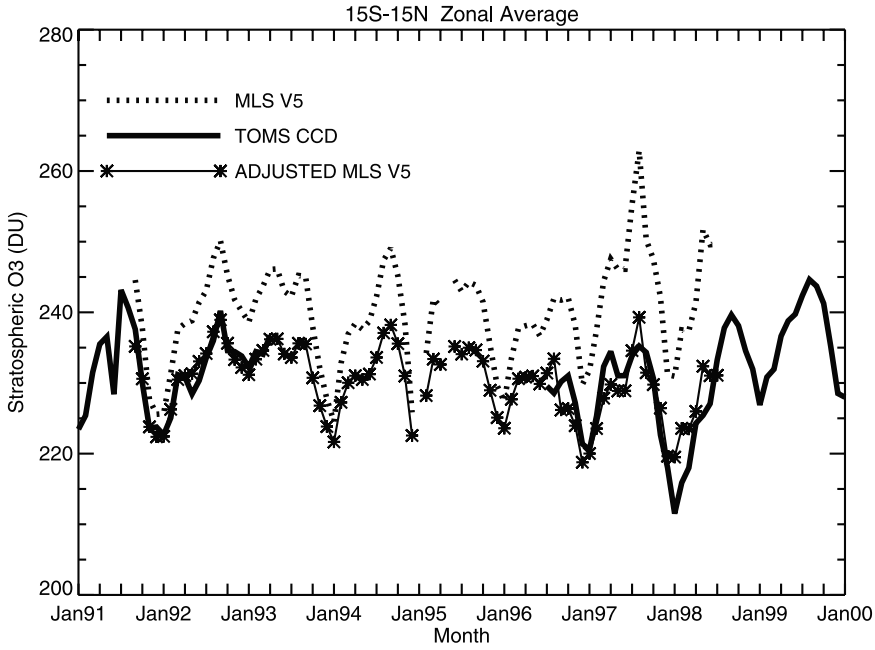

Figure 2. Same as Figure 1 but with HALOE replaced with normalized MLS version 5. stratospheric column ozone (stars). Normalization was accomplished by applying a first-order linear regression relationship to original MLS and original CCD SCO data: CCD = C1 + C2*MLS. Following the determination of the constants C1 and C2, the adjusted MLS SCO data is given by C1 + C2*MLS where MLS is the original MLS SCO data. Two normalization time periods were applied: (1) the Nimbus 7 time period September 1991–April 1993 (C1 = 70.5, C2 = 0.673), and (2) the Earth Probe time period August 1996–July 1998 (C1 = 76.4, C2 = 0.620). MLS stratospheric column ozone plotted in this figure from May 1993–July 1996 incorporated the Nimbus 7 normalization.

most 1–2 DU. This is particularly apparent during the Nimbus 7 time period. A relatively larger difference during the EP TOMS period after June 1997 is most likely due to the change in retrieval algorithm of the MLS v5 data after that time and noise caused by the poor coverage of the data.

4. Validation With Ozonesonde Measurements

[12] If we assume that the calibration bias of the MLS instrument with respect to TOMS is independent of geographical location, we can use the calibration developed from the tropical data to apply at all latitudes. This enables us to derive the global map of column ozone from ground to 100 hPa using concurrent measurements of ozone from TOMS and MLS instruments. In the tropics, the tropopause pressure is close to 100 hPa. Therefore, ground to 100 hPa column ozone is nearly equivalent to TCO. Outside the tropics, it is a combination of both TCO and lower stratospheric column ozone. We note that the CCD SCO measurements used to normalize MLS SCO are based on high-reflectivity (R > 0.9) scenes while TOMS total ozone measurements are based on low reflectivity (R < 0.2) clear-sky scenes. As stated by *Ziemke and Chandra* [1999], the low reflectivity total ozone measurements for EP TOMS appear to be biased with around +5 DU offset relative to Nimbus 7. This number is based on several years of comparisons with ozonesondes from WOUDC and SHADOZ and appears to be related to version 7 algorithms used in deriving total column ozone from EP TOMS using low reflectivity scenes. Because the normalization method uses only R > 0.9 scenes, this EP TOMS offset in derived TCO remains following residual differencing with clear-sky total ozone. In this study we subtracted 5 DU from the EP TOMS clear-sky total ozone measurements prior to determining TCO. Recently, TOMS data have been reprocessed (P. K. Bhartia, personal communication, 2002) using a new version 8 algorithm. A preliminary analysis of this data does not indicate a relative bias of EP TOMS with respect to Nimbus 7 column ozone measurements.

[13] Figure 3 compares the ground-to-100 hPa column ozone derived from the TOMS/MLS residual with ozonesonde during the 1996–1998 period at a number of tropical stations. These stations are operated under SHADOZ (Southern Hemisphere Additional Ozonesonde) program [*Thompson et al.*, 2003]. Two of these stations, Nairobi, Kenya (1°S, 37°E) and Ascension Island (8°S, 14°W) are in the Atlantic region outside the main burning region in southern Africa. The other two, Watukosek (8°S, 113°E) and Samoa (14°S, 170°W), are respectively in eastern Java and south Pacific regions. The sonde data from these stations have been compared with TCO derived from the CCD and GEOS-CHEM model of *Chandra et al.* [2002] and have been found to be in excellent agreement with both CCD and the model results. Figure 3 suggests similar agreement between sonde and TOMS/MLS residual. Many of the known characteristics of TCO in this region are well represented by both the data sets. They include a relatively large seasonal variation in the Atlantic region with peak values of 40–50 DU during austral spring and an increase of 10–20 DU in TCO at Watukosek during September–

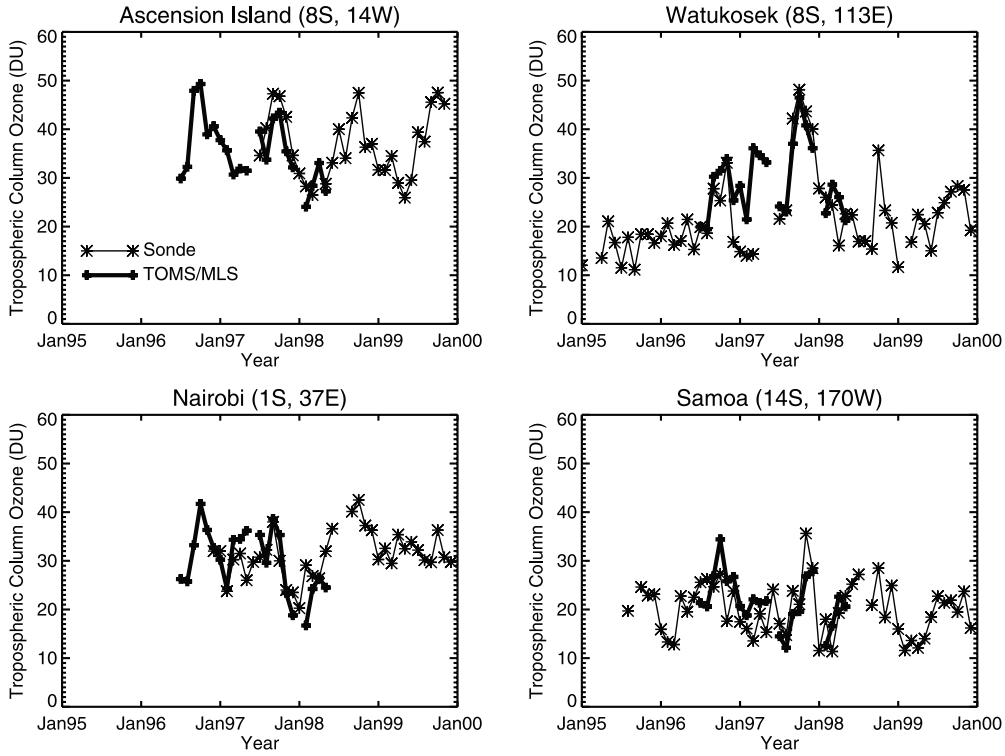

Figure 3. Tropospheric column ozone (in Dobson units) from ozonesonde at selected SHADOZ station sites (indicated in each frame). TOMS/MLS time series shown as bold with plus signs are column ozone from ground to 100 hPa. Ozonesonde time series are shown as light curves with stars.

October 1997 compared to the same months during 1996 [*Fujiwara et al.*, 1999]. This increase in TCO at Watukosek is caused by biomass burning and the change in dynamical conditions associated with the 1997 El Niño as discussed by *Chandra et al.* [2002]. The two data sets in Figure 3 are highly correlated. The correlation coefficient of the TOMS/MLS and sonde TCO based on the combined data from the four stations in Figure 3 is 0.78 which is highly significant. The relative bias of TOMS/MLS with respect to sonde for the same data sets is 3.4 DU and the RMS of their difference is 5.7 DU.

[14] Outside the tropics the tropopause pressure changes significantly with latitude and season (see Figure 6) and therefore column ozone from ground-to-100 hPa derived from TOMS/MLS contain more stratospheric contributions. Figure 4 compares seasonal variations in monthly means in ground-to-100 hPa column ozone inferred from TOMS/MLS residual and ozonesonde at a number of locations representative of high, middle, and low latitudes in both the northern and southern hemisphere. They are: Churchill, Canada (59°N, 94°W), Legionowo, Poland (53°N, 21°E), Hohenpeissenberg, Germany (48°N, 11°E), Boulder, Colorado (40°N, 105°W), Wallops Island, Virginia (38°N, 75°W), Tateno, Japan (36°N, 140°E), Kagoshima, Japan (32°N, 131°E), Naha, Japan (26°N, 128°E),Hilo, Hawaii (20°N, 155°W), Reunion Island (21°S, 55°E), Easter Island (27°S, 109°W) and Laverton, Australia (37°S, 145°E). Also shown in this figure are the TCO amounts (ground-to-tropopause) inferred from the sonde data. The ozone measurements from many of the sonde locations are based on almost 9 years of measurements from 1991 to 1999. In comparison, MLS data represent an average of mostly 1991–1992 and 1996–1997 time periods. Because of the yaw maneuver, the MLS measurements at higher latitudes (>30°) are relatively sparse compared to low latitudes (<30°). The two datasets, nevertheless, show good agreement in capturing the seasonal variations in the ground-to-100 hPa column ozone at most locations. These comparisons give general support to the assumption that the calibration bias of the MLS instrument with respect to TOMS is independent of geographic locations.

[15] The peak values inferred from both data sets tend to vary from 80–100 DU at Churchill and Hohenpeissenberg to about 50 DU at Hilo. The seasonal cycles at all northern latitude stations are similar with maximum values during spring and minimum values during fall and summer months. Unfortunately, the network of sonde stations in the southern hemisphere outside the tropics is not as extensive as in the northern hemisphere. However, the last three stations (Reunion Island, Easter Island, and Laverton) in Figure 4, which are low and midlatitude stations in the southern hemisphere, show seasonal patterns similar to the northern hemisphere but with a phase shift of about 6 months. The sonde measurements at Laverton show a relatively larger bias with respect to TOMS/MLS compared to stations at northern midlatitudes. It is not clear if this is a local or a regional problem. Figure 4 also indicates a significantly larger stratospheric contribution at high latitudes (>40°) and almost no contribution at low latitudes (<20°). At middle latitudes (20°–40°) the stratospheric contribution is seasonally dependent with maximum contribution during winter and spring months. Most of these are due to changes in

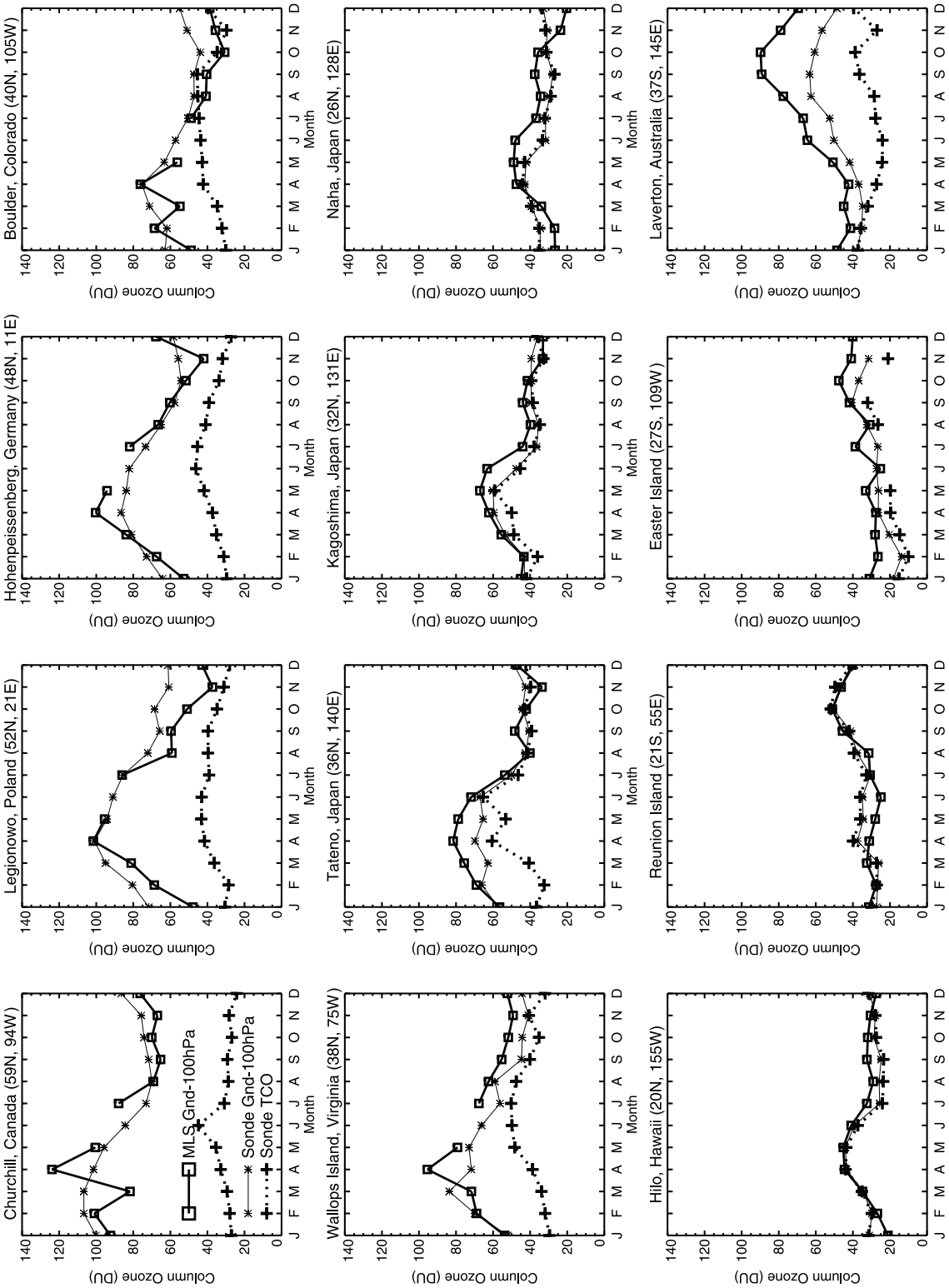

Figure 4. Seasonal cycles in ground-to-100 hPa column ozone (in Dobson units) for TOMS/MLS (squares) and ozonesonde (stars) at WOUDC sonde sites (indicated). Also plotted in each frame (dotted curves) are seasonal cycles in ozonesonde TCO. All seasonal cycles were calculated for 1992–1998.

Table 1. Relative Bias, RMS, and r Values of Column Ozone From Ground to 100 hPa for TOMS/MLS and Ozonesonde

Station	TOMS/MLS-Sonde, DU	RMS, DU	r
Churchill (59N, 94W)	−2.3	11.6	0.75
Legionowo (52N, 21E)	−12.6	14.1	0.96
Hohenpeissenberg (48N, 11E)	−0.3	8.5	0.90
Boulder (40N, 105W)	−9.5	11.7	0.85
Wallops Island (38N, 75W)	4.6	9.5	0.83
Tateno (36N, 140E)	1.9	6.5	0.94
Kagoshima (32N, 131E)	0.5	5.4	0.85
Naha (26N, 128E)	−0.1	8.2	0.40
Hilo (20N, 155W)	−0.1	4.4	0.78
Reunion Island (21S, 55E)	−0.5	5.1	0.80
Easter Island (27S, 109W)	8.0	9.3	0.73
Laverton (37S, 145E)	17.6	19.5	0.97

tropopause height at middle and high latitudes. Table 1 gives the relative bias of TOMS/MLS with respect to sonde for the 12 stations in Figure 4. Shown in this table are also the root mean square (RMS) values of their difference and their correlation coefficient (r). Table 1 shows good correlation between TOMS/MLS and sonde data at all locations except Naha. Their relative bias tends to be low (< 4 DU) except for some of the higher-latitude stations, e.g., Legionowo, Boulder, and Laverton.

5. High-Resolution Global Maps

[16] Figures 5a and 5b show examples of high-resolution (1° × 1°) global maps of ozone column from ground to 100 hPa that can be produced on almost a daily basis from September 1991 to May 1993 using TOMS/MLS residual. Daily maps are more difficult to obtain for the 1996–1998 period since the temporal coverage of the MLS data was reduced to only a few days per month during that period. Prior to differencing with 1° × 1° TOMS, a two-dimensional (latitude, longitude) interpolation scheme was applied to MLS data to obtain 1° × 1° gridded 0–100 hPa column ozone fields. Figures 5a and 5b each correspond to 5-day averages separated by one week and centered on September 17 and September 24, 1992. A linear correction method for aerosols [*Torres and Bhartia*, 1999] was applied to all TOMS total ozone measurements in this study. This correction also provides partial adjustment for scan-angle errors associated with sea glint (i.e., bright surface reflection over ocean) in which daily total ozone measurements may be underdetermined by up to 10 to 15 DU. The 5-day averaging applied to the ozone data smooths out remaining scan-angle bias errors caused by sea glint and also fills in missing data in the tropics caused by orbital gaps. In Figures 5a and 5b the two large dark bands (northward of around 30°N in Figure 5a and southward of around 30°S in Figure 5b) are regions where there were no MLS measurements during the days shown because of the satellite yaw maneuver. There are additional missing data in Figures 5a and 5b because all TOMS total column ozone measurements are filtered for low reflectivity (R < 0.2) scenes to avoid errors associated with clouds. The impact of missing data caused by clouds is most apparent in the Southern Hemisphere in Figure 5a. Other regions with persistent clouds include the west coast

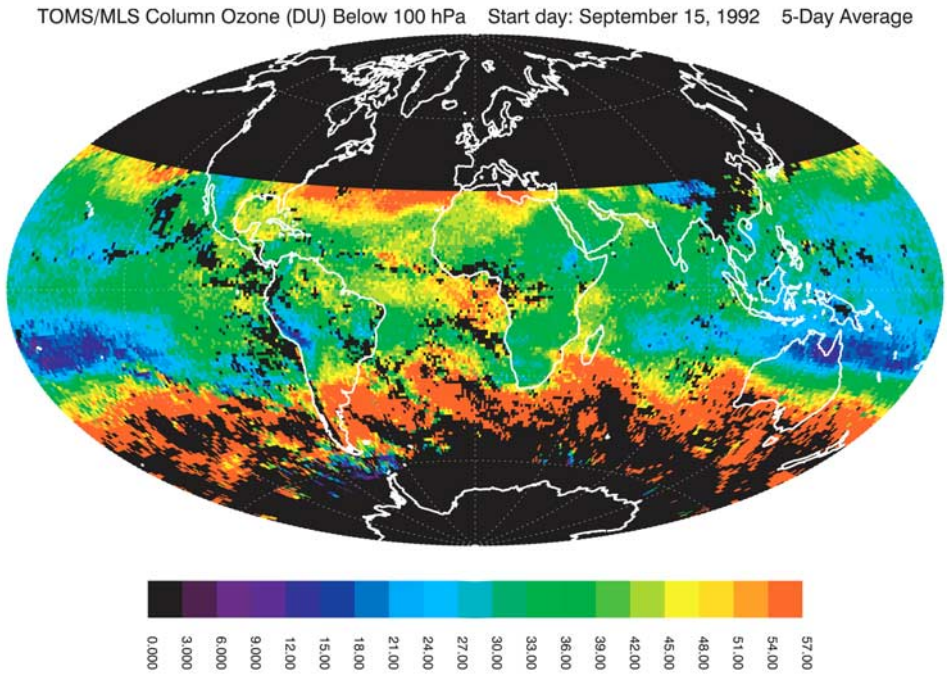

Figure 5a. High-resolution (1° × 1°) TOMS/MLS ground-to-100 hPa column ozone averaged over September 15–19, 1992. Bottom color bar designates column amount in Dobson units. Column amounts greater than 54 Dobson units are saturated as red color. Black regions are flagged as missing data due to the presence of persistent clouds. Large black band in NH designates no available MLS data due to UARS yaw maneuver. The data were averaged over 5 days to smooth out existing scan-angle bias and missing data gaps in the low latitudes for Nimbus 7 TOMS.

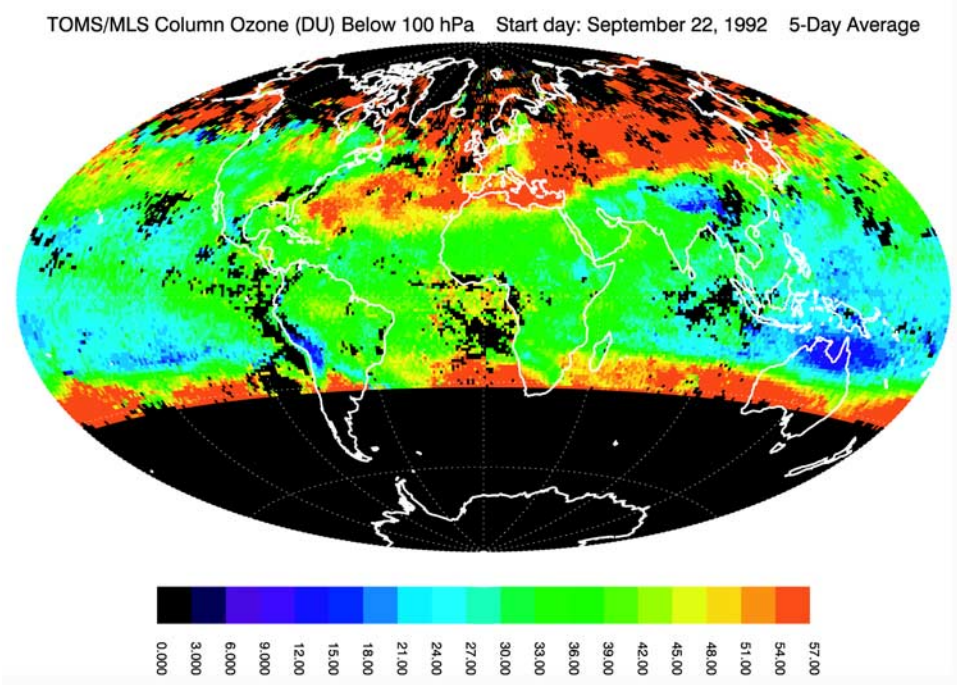

Figure 5b. Same as Figure 5a but for September 22–26, 1992.

of South America and Central America, the equatorial Atlantic, and eastern Asia.

[17] Despite limitations of the combined TOMS and MLS measurements, Figures 5a and 5b highlight numerous details regarding both ozone properties and the meteorological conditions present. The changes in tropopause pressure are most pronounced in regions associated with the upper tropospheric wind jets. At midlatitudes, the wind jets can be identified from color gradients that change from green (~40 DU) to yellow (~50 DU) to orange (> 50 DU). The wind jet regions are more easily identified in the Southern Hemisphere and appear as the boundary of the meandering orange wave pattern in Figure 5a. Poleward of the wind jets the tropopause pressure increases rapidly.

[18] The two maps in Figures 5a and 5b essentially show both the spatial and temporal changes in TCO between ±30° where the tropopause is close 100 hPa. They show well-known features of elevated ozone (40–50 DU) in the tropics encompassing the regions between South America and southern Africa [e.g., *Chandra et al.*, 2002]. The tropical enhancement during this time is usually attributed to biomass burning in southern Africa and Brazil. However, the elevated ozone occurs over most of the Atlantic Ocean south of the equator and not over land where the biomass burning takes place. Ozone is also elevated over regions north and south of 30° latitude. Most of this increase may be attributed to increased stratospheric contribution as indicated in Figure 4.

[19] Figures 5a and 5b depict several other features such as persistent low ozone over mountainous regions such as Andes and Himalayas (down to values less than 10 DU). Low ozone values in these regions are topographically induced. The high ozone in the Atlantic exhibits a plume stretching toward South America as observed during the TRACE-A experiment [*Fishman et al.*, 1996]. Also larger amounts occur for September 15–19 when compared to September 22–26. The rapid loss of ozone over only one week time period in the Atlantic suggests that much of the ozone may have been in the low to middle troposphere where rapid ozone destruction occurs [*Jacob et al.*, 1996; *Thompson et al.*, 1996].

6. Tropospheric Column Ozone (TCO) From TOMS/MLS Residual

[20] In order to calculate TCO from TOMS/MLS residual, it is necessary to account for the excess ozone ΔO_3 between the tropopause and 100 hPa. Over most of the tropical latitudes this is not a problem since the tropopause is close to 100 hPa. The tropopause does not deviate significantly from 100 hPa over latitudes between ±30° and a simple correction can be made for ΔO_3. Figure 6 shows a climatology of zonal mean tropopause pressure (TP) derived from seven years (1992–1998) of National Centers for Environmental Prediction (NCEP) temperature profiles, using the World Meteorological Organization criterion [e.g., *Logan*, 1999, and references therein] of determining tropopause. According to this criterion the tropopause is defined as the lowest level at which the temperature lapse rate decreases to 2K/km or less provided the average lapse rate between this level and all higher levels within the next 2 km does not exceed 2K/km. The tropopause calculated from the WMO definition does not differ significantly from the cold-point tropopause definition over most of the tropical and low latitudes, but the WMO tropopause pressure can be up to 40 hPa greater than the cold-point tropopause pressure near 30°N. The latter is defined as the pressure at which temperature

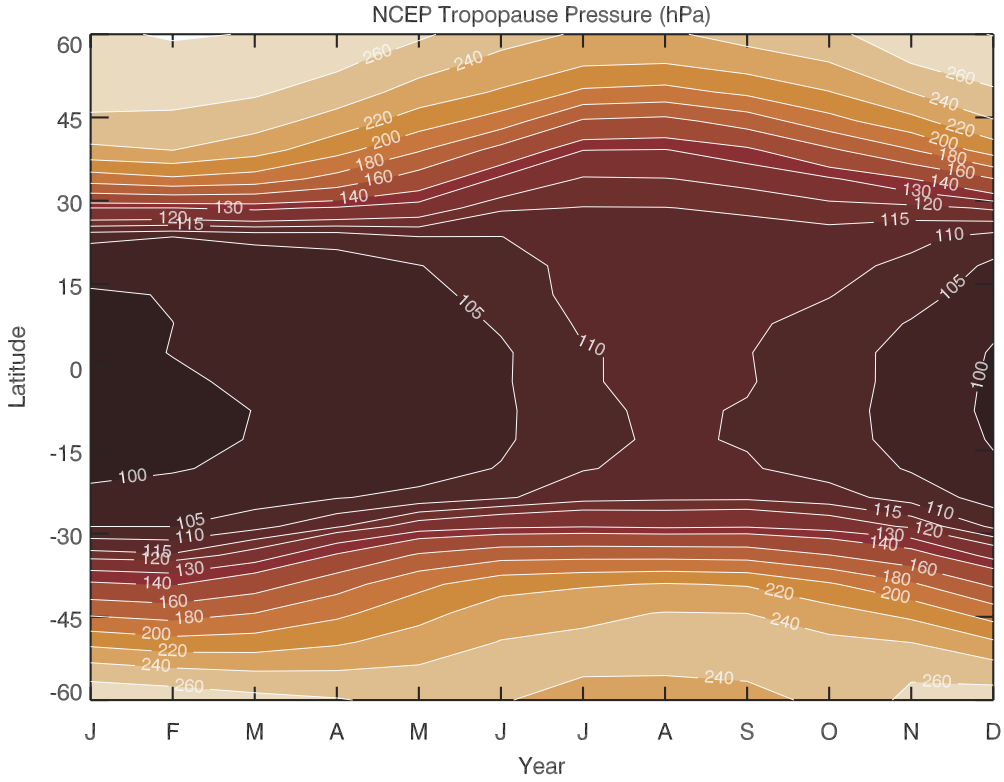

Figure 6. Zonal mean NCEP tropopause pressures (units hPa) averaged over the years 1992–1998. Tropopause pressures were calculated from NCEP reanalyses using the WMO 2K km^{-1} tropopause pressure definition (discussed in text).

reaches minimum value between the troposphere and the stratosphere. The TP climatology in Figure 6 shows a relatively constant value near 100 hPa in the tropics and increases gradually to about 120–130 hPa at 30°S and 30°N. Outside this latitude range, TP shows a strong latitudinal gradient increasing rapidly to 240–260 hPa towards high latitudes (50°–60°). It also shows a strong seasonal variation with increasing latitude with peak values during spring months in both hemispheres. These features are similar to TP changes inferred from sonde data [*Logan*, 1999] and are reflected in seasonal characteristics of ozone amount between the tropopause and 100 hPa at middle and high latitudes as in Figure 4.

[21] For TP greater than 100 hPa, a first order correction can be made using an empirical relation between ΔO_3 and ΔP (the difference between TP and 100 hPa level). Figure 7 shows a scatterplot of ΔO_3 versus ΔP. Both quantities are calculated from sonde-based ozone and temperature profiles measured simultaneously at several locations including those used in Figures 3 and 4. Figure 7 also shows a least squares parabolic fit of the scatterplots using the following relation:

$$\Delta O_3 = c1\Delta P + c2\Delta P^2 \quad (1)$$

where c1 = 0.190 and c2 = 0.000871. Figure 7 shows a monotonic increase in ΔO_3 with respect to ΔP with relatively smaller scatter (~5 DU) with respect to the regression line for $\Delta P < 100$ hPa (e.g., TP < 200 hPa). These points correspond mostly to latitudes equatorward of 40°. In this region the TOMS/MLS residual values can be corrected for stratospheric contribution by estimating ΔP from the NCEP analyses and applying (1). The scatter becomes significantly large for higher values of ΔP (>100 hPa), which mostly correspond to latitudes poleward of 40°. In this region the correction using (1) may lead to large uncertainty in TCO.

[22] Figure 8 compares the seasonal variations in TCO from TOMS/MLS and sonde after correcting TOMS/MLS residual data for ΔO_3. Figure 8 is similar to Figure 4 except the column values from ground to 100 hPa are replaced by column values from ground to tropopause. In general, the two time series track each other quite well with no significant bias over most of the locations. This is also indicated in Table 2, which lists their relative bias, RMS values and correlation coefficients as in Table 1. The exceptions are two high-latitude sites, Legionowo and Boulder, and one sub-tropical site, Easter Island. The TOMS/MLS bias with respect to sonde at these sites are respectively −6.2, −15.5 and 11.5 DU. It is interesting to note that a relatively larger bias at Laverton (17.6 DU) before the correction (Table 1) is reduced to 0.5 DU after accounting for ΔO_3.

7. Error Estimate

[23] Because of the nature of cross-calibrating SCO measurements from TOMS and MLS, absolute measurement errors with either TOMS or MLS have little impact in affecting the derived TCO residual. However significant errors may be traced to uncertainties in calculated normal-

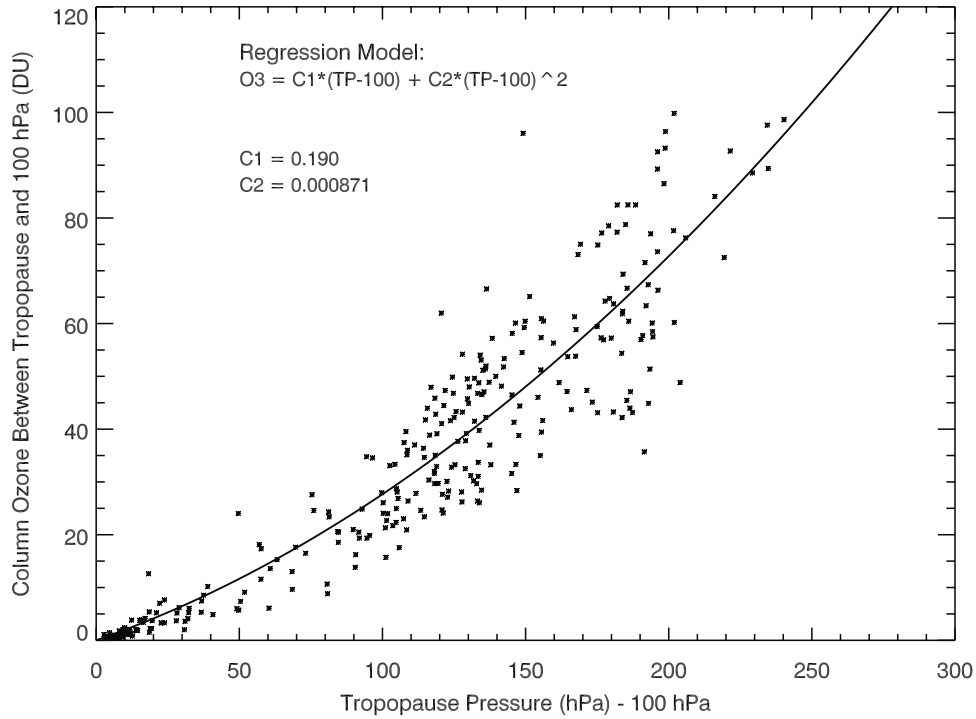

Figure 7. Scatterplot of column ozone between tropopause and 100 hPa (ΔO_3) versus the difference of tropopause pressure minus 100 hPa (ΔP). Both ΔO_3 along vertical axis (in Dobson units) and ΔP along horizontal axis (in hPa) were calculated from sonde-based ozone and temperature profiles measured simultaneously at the locations shown in Figures 5a and 5b. The tropopause pressure was calculated from temperature profiles using the cold point definition. Also shown in this figure is a least squares parabolic fit of the scatterplot using the regression relation $\Delta O_3 = C1 \cdot \Delta P + C2 \cdot \Delta P^2$ where C1 = 0.190 and C2 = 0.000871. The statistical 2σ value for C1 is 0.0367 and for C2 it is 0.000222 (see text for discussion of regression method).

ization coefficients. Another source of error in TCO is the ozonesonde regression adjustment (Figure 7) made for tropopause pressures deviating from 100 hPa at latitudes between ±30°. While it is possible to quantify all of these errors from statistical uncertainties in the regression coefficients, we have opted instead to compare the final derived values of TOMS/MLS ground-to-100 hPa column ozone with similar measurements from ozonesondes by calculating 2σ differences (σ being one standard deviation) assuming ozonesonde data as truth. Because the tropopause is consistently around 100–110 hPa year-round in the tropics, the ground-to-100 hPa column amount in the tropics is equivalent to TCO within 1–2 DU.

[24] The TCO validation in this study involved comparisons of both 1998 tropical SHADOZ and pre-SHADOZ (prior to 1998) WOUDC tropical and extratropical ozonesonde measurements. Because Nimbus 7 and EP TOMS data are from different time periods, separate regression calibrations/normalizations were invoked. The SHADOZ and WOUDC ozonesonde data were compared independently with TOMS/MLS TCO for the Nimbus 7 and EP TOMS time periods. Also, independent tropical and extratropical (extending to ±40° latitude) comparisons were made for both Nimbus 7 and EP TOMS. For the tropics, WOUDC ozonesonde data from Ascension Island (8S, 14W) and Brazzaville (4S, 15E) for the Nimbus 7 time period were available for comparison during September 1991–October 1992 and indicated an average 2σ error of 3.5 DU. In the tropics, 11 stations sites for SHADOZ and WOUDC ozonesondes (including the SHADOZ sites plotted in Figure 3) for August 1996 through 1998 indicated an average 2σ value of 4 DU for the EP TOMS time period. For the extratropics extending to ±40° latitude (i.e., encompassing the subtropics in both hemispheres), ground-to-100 hPa column ozone for both Nimbus 7 and Earth Probe time periods were compared with similar measurements from WOUDC ozonesondes at 7 station sites.

[25] For the Nimbus 7 time period, ground-to-100 hPa column ozone up to latitudes ±40° showed an average 2σ value of 6 DU. For the EP TOMS time period an average 2σ error of 8 DU was indicated. When WOUDC data were extended only to ±35° latitudes the 2σ values for both Nimbus 7 and EP TOMS were around 5 DU. In this study we analyze only TCO data equatorward of ±30° latitude. In summary, ozonesonde comparisons indicate that an estimate for 2σ uncertainty in local TCO measurements for either Nimbus 7 or EP TOMS time periods is 5 DU for these latitudes.

8. Zonal Variability in TCO and SCO

[26] One of the basic assumptions in deriving TCO from the CCD method was to assume that SCO estimated from high reflecting clouds in the Pacific was zonally invariant within 5 DU over all tropical latitudes. This assumption was based on stratospheric ozone data from SAGE [*Fishman et al.*, 1990; *Shiotani and Hasebe*, 1994], MLS [*Ziemke et al.*,

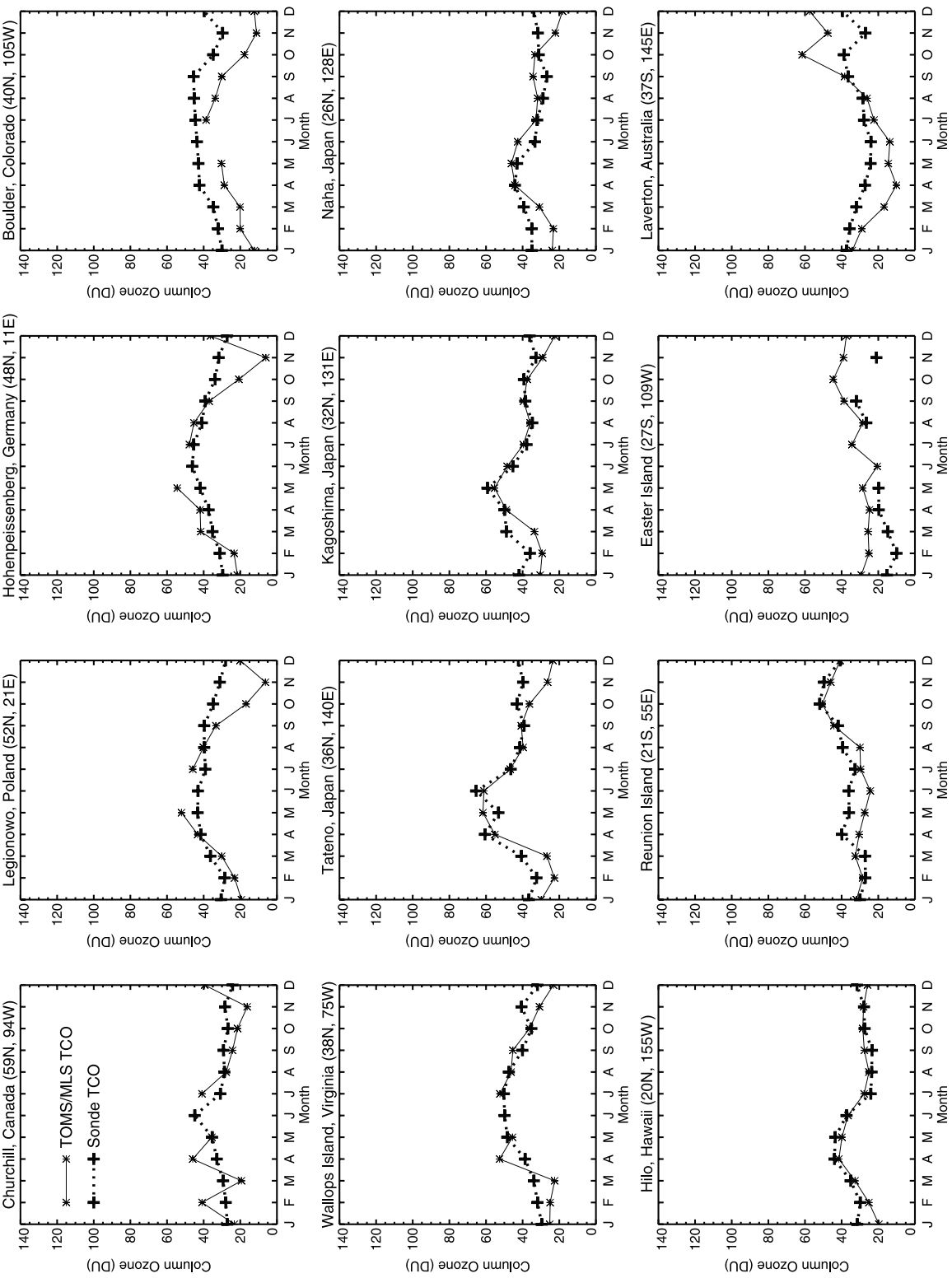

Figure 8. Seasonal cycles in TCO for TOMS/MLS (squares) and ozonesonde (stars) at WOUDC sonde sites (indicated) as in Figure 4.

Table 2. Same as Table 1 Except for Column Ozone From Ground to Tropopause (TCO)

Station	TOMS/MLS-Sonde, DU	RMS, DU	r
Churchill (59N, 94W)	0.0	9.5	0.30
Legionowo (52N, 21E)	−6.2	11.1	0.85
Hohenpeissenberg (48N, 11E)	−2.4	10.8	0.70
Boulder (40N, 105W)	−15.5	15.9	0.85
Wallops Island (38N, 75W)	−3.0	7.4	0.81
Tateno (36N, 140E)	−5.9	9.3	0.87
Kagoshima (32N, 131E)	−4.2	7.4	0.76
Naha (26N, 128E)	−2.6	8.4	0.43
Hilo (20N, 155W)	−1.7	4.6	0.79
Reunion Island (21S, 55E)	−3.0	6.2	0.77
Easter Island (27S, 109W)	11.5	11.3	0.64
Laverton (37S, 145E)	−0.5	13.2	0.72

1996], and MLS and HALOE [*Ziemke et al.*, 1998]. More recently the zonal invariance of SCO in the tropics was corroborated from ozonesonde measurements from SHADOZ [*Thompson et al.*, 2003]. Figures 9a and 9b (lower panels) suggest that SCO is zonally invariant within this range not only in the tropics but also to within 10 DU outside the tropics extending to about 30° latitude in both hemispheres. These figures also compare zonal variability in TCO derived from the CCD method assuming a zonally invariant stratosphere (upper panels) with TCO derived from the TOMS/MLS residual. The latter implicitly accounts for the zonal variability in SCO. Figures 9a and 9b are based on September 1991 and February 1997 data. They suggest that the zonal characteristics of TCO derived from the CCD method are similar to those derived from the TOMS/MLS residual method within the uncertainty of the zonal variability of SCO. In the latitude region between 10°N and 10°S, the zonal correlation of TOMS/MLS and CCD for September 1991 is 0.9, their relative bias (TOMS/MLS-CCD) is −1.9 DU and the RMS of their difference is 4.1 DU. For February 1997, the corresponding values are respectively 0.94, −0.8 DU and 2.1 DU.

[27] Both Figures 9a and 9b show a predominant wave one feature in the tropics with maximum values in the Atlantic and minimum values in the Pacific. Outside the tropics, the wave one features in the troposphere weaken

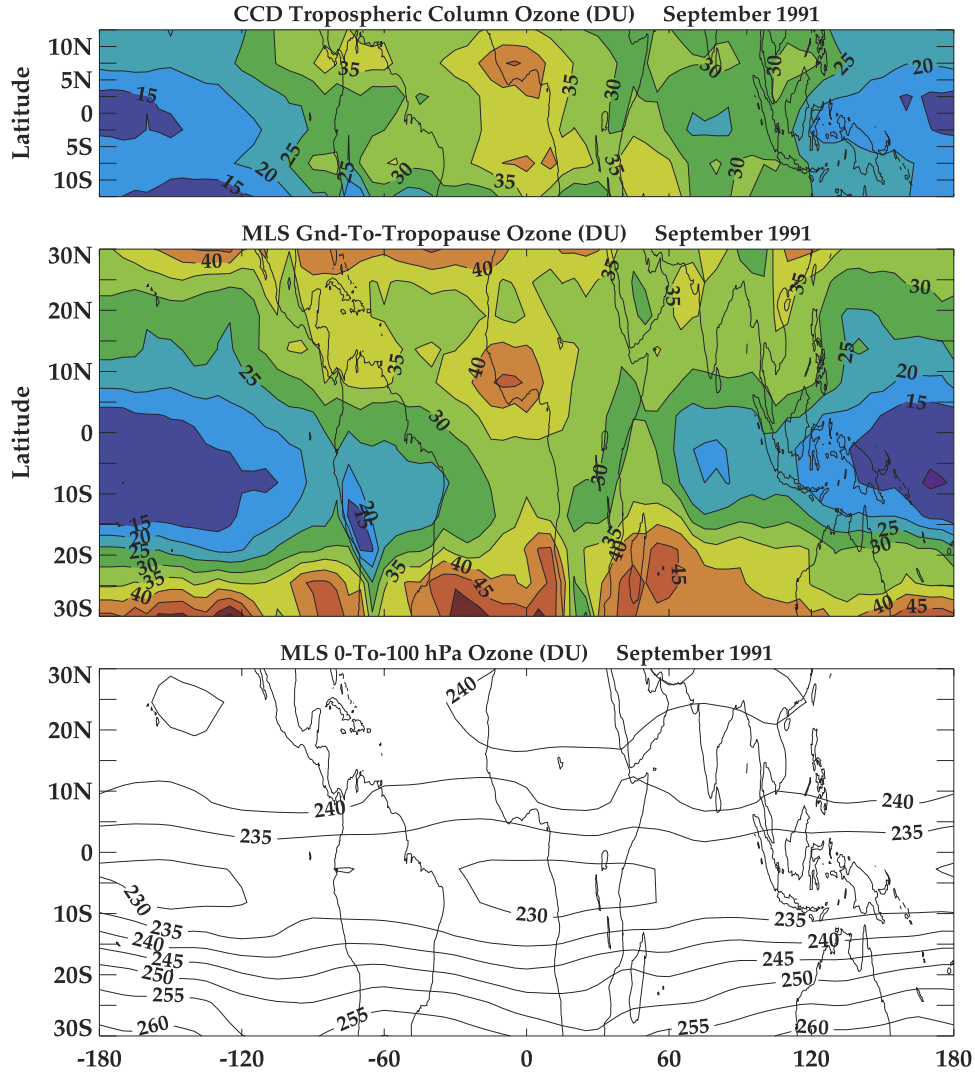

Figure 9a. Top: Monthly mean CCD TCO for September, 1991. Middle: Monthly mean TOMS/MLS TCO for September 1991. Bottom: Monthly mean MLS SCO for September 1991.

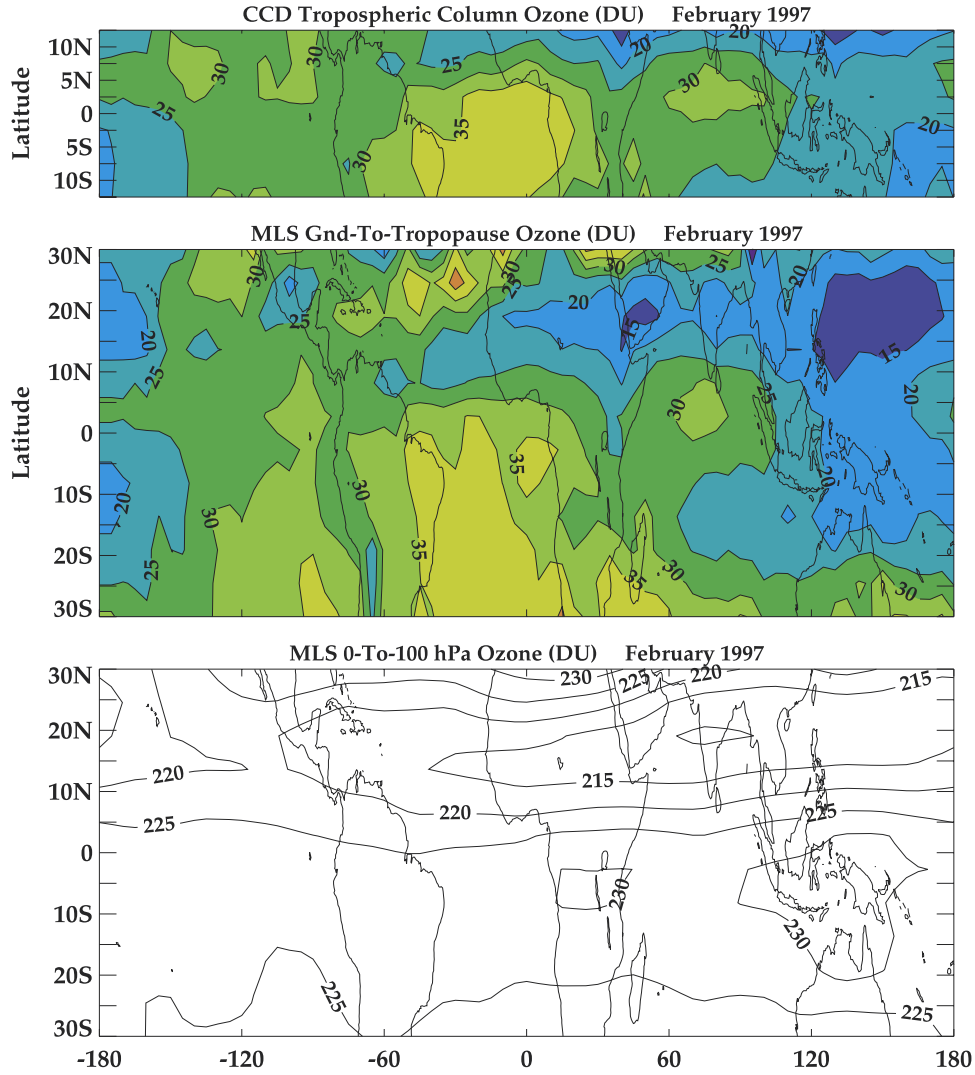

Figure 9b. Same as Figure 9a but for February 1997.

considerably. The decline of the wave 1 pattern outside the tropics is associated with a decline in lightning activity and Walker circulation as indicated from the GEOS-CHEM model (section 9).

[28] The zonal characteristics of SCO, inferred from Figures 9a and 9b, are typical of the entire data sets based on TOMS/MLS residual including the El Nino years. Even though they show significant latitudinal and seasonal variability, their zonal variability is generally less than 5 DU at tropical and sub-tropical latitudes with no specific zonal pattern. They do not support the conclusions of *Newchurch et al.* [2001] about the presence of a wave one in SCO with about 8–10 DU increase from the Pacific to the Atlantic region. The conclusions by *Newchurch et al.* [2001] were based on data from Nimbus 7 TOMS and the Nimbus 7 Temperature Humidity Infrared (THIR) sensor. These authors questioned the conclusions based on MLS, HALOE and SAGE data because of profile measurement uncertainties from these instruments below 68 hPa and the poor spatial sampling of the observational data from limb scanning satellite instruments of HALOE and SAGE. These arguments do not seem to be valid, since SCO is a column integral from 100 hPa to the top of the atmosphere and the contribution to SCO from the region between 68–100 hPa is only about 2–3 percent (~6–8 DU) [*Ziemke et al.*, 1996]. It is not likely to introduce an error in the column amount significant enough to produce a an 8–10 DU peak-to-peak zonal wave 1 in SCO. In addition, RMS uncertainties in SCO as shown by *Newchurch et al.* [2001] are as large as the measurements of derived SCO, and the data sampling from the technique is unfortunately limited in the tropics, as much if not more limited than either SAGE or HALOE occultation measurements. Current investigation of the TOMS/THIR method (M. Newchurch and Z. Ahmad, personal communication, 2002) suggests that the increases in SCO over the Atlantic (mostly observed increases over South America and African land masses shown by *Newchurch et al.* [2001]) may be attributed to multiple-scattering of UV within highly reflecting convective clouds (reflectivity R > 0.8) in the presence of large ozone content in the upper troposphere within the cloud tops. This scattering does not appear to affect the CCD measurements of *Ziemke et al.* [1998] since SCO is determined over the Pacific where ozone content in the upper troposphere is

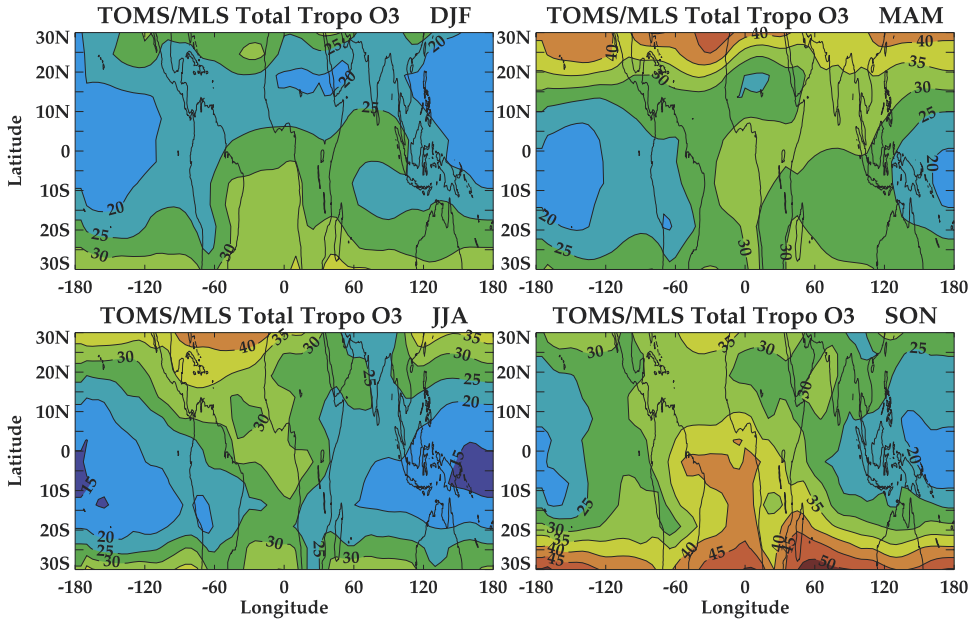

Figure 10. TOMS/MLS TCO seasonal averages (indicated) from combined Nimbus 7 (September 1991–April 1993) and Earth Probe (August 1996–December 1998) measurements. Column amounts shown are in Dobson units.

generally small compared to the Atlantic region [*Kley et al.*, 1996].

9. Comparison With the GEOS-CHEM Model

[29] As discussed by *Chandra et al.* [2002] and *Martin et al.* [2002] and noted earlier in the introduction, the zonal and seasonal characteristics of TCO derived from the CCD method during the 1996–1997 period are well represented by the GEOS-CHEM model at tropical latitudes south of the equator. The agreement, however, breaks down north of the equator over sub-Saharan northern Africa where the seasonal variations in model and observation tend to be out of phase. The TCO data obtained from TOMS/MLS allows the comparison of GEOS-CHEM model well outside the tropics where sonde data can be used for cross validation. In the following, we will make some of these comparisons and discuss their implications.

[30] The GEOS-CHEM model was initially described by *Bey et al.* [2001a]. Subsequent improvements are described by *Martin et al.* [2002]. The model is driven by assimilated meteorological data updated every 3–6 hours from the Global Earth Observing System (GEOS) of the NASA Data Assimilation Office (DAO) [*Schubert et al.*, 1993]. We use for this study the GEOS data for 1996–97, available with a resolution of 2° latitude by 2.5° longitude and 46 sigma levels in the vertical extending up to 0.1 hPa. For computational expedience we degrade the horizontal resolution to 4° latitude by 5° longitude and merge the vertical levels above the lower stratosphere, retaining a total of 26. We conduct simulations from March 1996 through November 1997. The first six months are used to achieve proper initialization. We present results for September 1996 through November 1997.

[31] The GEOS-CHEM model includes a detailed description of tropospheric O_3-NO_x-hydrocarbon chemistry. It solves the chemical evolution of about 120 species with a Gear solver [*Jacobson and Turco*, 1994] and transports 24 tracers. Photolysis frequencies are computed using the Fast-J radiative transfer algorithm [*Wild et al.*, 2000], which includes Rayleigh scattering as well as Mie scattering by clouds and mineral dust. The tropopause in the model is determined using the World Meteorological Organization standard criterion of a 2 K km^{-1} lapse rate. The cross-tropopause transport of ozone is simulated by the Synoz (synthetic ozone) method [*McLinden et al.*, 2000] using their recommended flux of 475 Tg O_3 yr^{-1}.

[32] Emissions of NO_x from lightning are 6 Tg N yr^{-1} and linked to deep convection following the parameterization of *Price and Rind* [1992] as implemented by *Wang et al.* [1998]. Biogenic isoprene and NO_x emissions from land are computed locally using modified versions of the *Guenther et al.* [1995] and *Yienger and Levy* [1995] algorithms, as described by *Wang et al.* [1998] and *Bey et al.* [2001a]. Interannual variability in biomass burning emissions is determined from satellite observations as described by *Duncan et al.* [2003]. Extensive evaluations of the GEOS-CHEM ozone fields with observations are presented in a number of papers [*Bey et al.*, 2001a, 2001b; *Chandra et al.*, 2002; *Fiore et al.*, 2002; *Li et al.*, 2001, 2002a, 2002b; *Liu et al.*, 2002; *Martin et al.*, 2002, 2003].

[33] Figure 10 shows zonal variations in TCO climatology between ±30° based on TOMS/MLS data. The four panels in this figure are averages of December–January–February (DJF), March–April–May (MAM), June–July–August (JJA), and September–October–November (SON). The seasonal and zonal characteristics of TCO in the tropics inferred from Figure 10 are similar to the ones discussed by *Chandra et al.* [2002] based on the CCD data. They show a predominantly zonal asymmetry in all seasons with maximum TCO values in the Atlantic and minimum in the Pacific region. The origin of wave 1 in TCO has been attributed mostly to upper tropospheric ozone production

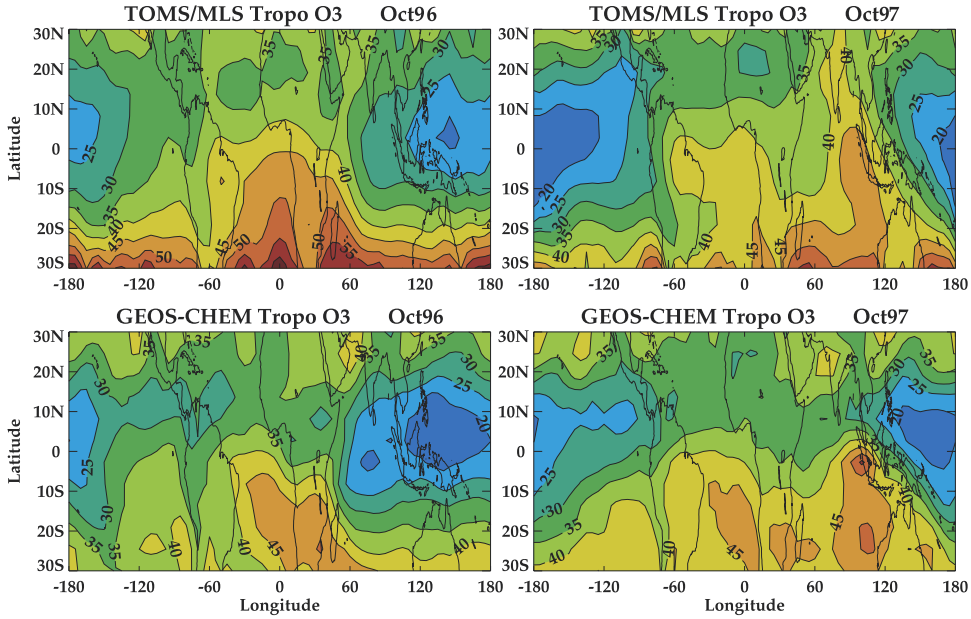

Figure 11. Top frames: TOMS/MLS TCO for October 1996 (left) and October 1997 (right). Bottom frames: GEOS-CHEM modeled TCO for October 1996 (left) and October 1997 (right). Column amounts shown are in Dobson units.

from lightning NO_x and biomass burning coupled with the large-scale Walker Circulation [*Moxim and Levy*, 2000; *Martin et al.*, 2002]. The seasonal contrast is greatest in the Atlantic with maximum values during austral spring over the southern tropical Atlantic. The high values of TCO in this region during austral spring have been attributed to biomass burning, lightning, and dynamics as part of TRACE-A [*Krishnamurti et al.*, 1993, 1996; *Jacob et al.*, 1996; *Pickering et al.*, 1996; *Thompson et al.*, 1996]. Outside the tropics, the zonal contrast decreases but seasonal contrast intensifies over all longitudes. The springtime enhancement of 10–20 DU over and downwind of Southeast Asia reflects a combination of downward transport from the stratosphere and biomass burning [*Liu et al.*, 1999]. In the northern hemisphere (20°N–30°N), TCO reaches peak values (40–45 DU) in spring (MAM) and summer (JJA) months and minimum values (20–25 DU) in winter months (DJF). In the southern hemisphere (20°S–30°S) a similar pattern is repeated with a phase shift of about 6 months. Over most of the tropical latitudes (15°N–15°S) encompassing South American and African continents, the seasonal characteristics of TCO are similar to those in southern hemisphere.

[34] Figure 11 compares zonal variations in TCO derived from the TOMS/MLS residual with GEOS-CHEM model for latitudes between ±30°. The comparison is made for October 1996 (the year before El Niño) and October 1997 (El Niño year). Similar comparisons were made by *Chandra et al.* [2002] between the GEOS-CHEM model and the TCO derived from the CCD method, but that comparison was limited to ±15°. As given by *Chandra et al.* [2002], the GEOS-CHEM model captures most of the observed characteristics of TCO derived from the TOMS/MLS residual. Some of these characteristics include a wave 1 like structure in the tropics with peak-to-peak values of 10–15 DU during October 1996, and an increase of about 15 to 20 DU in the Indonesian region from October 1996 to October 1997 associated with biomass burning and changes in dynamical condition caused by El Niño. Over most of the regions including northern Africa, model and observations agree within 5 DU. However, larger differences are seen between 20°S and 30°S during October 1996 where observed values are about 5–10 DU higher than the model values. In comparison the observed and modeled differences in October 1997 are about 5 DU and are statistically not significant. The differences between the data and the model for October 1996 and October 1997 are quantified in Tables 3 and 4.

[35] The differences between model and observations are more apparent during winter than during summer. Figure 12 compares the summer and winter differences between model and observations using February and July 1997 as

Table 3. Relative Bias, RMS in DU, and r Values of TCO for TOMS/MLS and Model for Selected Latitude Bands in Figure 11 for October 1996

Latitudes	TOMS/MLS-Model	RMS	r
20N–30N	−0.2	3.5	0.43
10N–20N	2.2	3.5	0.78
0N–10N	4.7	5.5	0.90
0S–10S	3.7	5.6	0.86
10S–20S	4.1	5.1	0.88
20S–30S	11.3	12.7	0.29

Table 4. Same as Table 3 but for October 1997 in Figure 11

Latitudes	TOMS/MLS-Model	RMS	r
20N–30N	−0.3	3.6	0.51
10N–20N	0.4	3.8	0.70
0N–10N	3.6	6.1	0.83
0S–10S	−1.7	4.4	0.90
10S–20S	−3.2	4.7	0.85
20S–30S	2.7	5.4	0.42

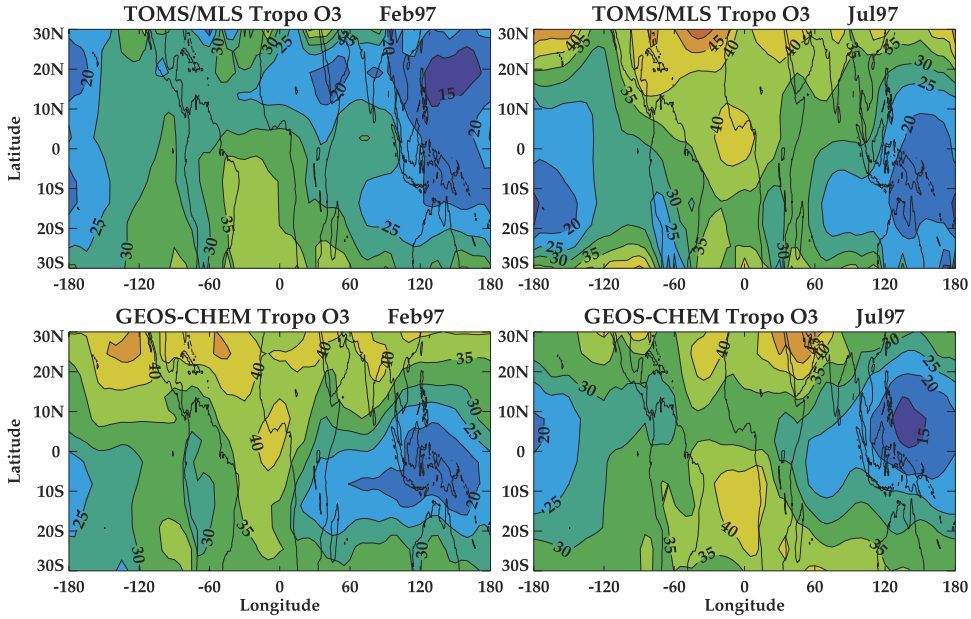

Figure 12. Top frames: TOMS/MLS TCO for February 1997 (left) and July 1997 (right). Bottom frames: GEOS-CHEM modeled TCO for February 1997 (left) and July 1997 (right). Column amounts shown are in Dobson units.

examples. For February, Figure 12 (left panels) indicates general agreement between model and observations south of the equator (southern summer) but significant differences (10–15 DU) north of equator. These differences are not limited to sub-Saharan northern Africa as discussed by *Martin et al.* [2002] but extend over most of the northern latitudes including Hawaii, Central America, Southeast Asia and the southern part of Japan. Over this entire region TOMS/MLS values are significantly lower than the model values. Ozone over the northern tropical Pacific during February 1997 exhibits particularly low ozone columns of 15 DU as indicated in Table 5.

[36] In comparison, the model and observations agree reasonably well in July (Figure 12, right panels) over most of the regions north of 15° where summer conditions prevail. The comparison of TOMS/MLS and GEOS-CHEM model in July is particularly noteworthy in the light of a recent model prediction [*Li et al.*, 2001] of a regional ozone maximum in the upper troposphere over the Middle East region. The model shows elevated values of TCO in the range of 40–45 DU. *Li et al.* [2001] have attributed these high values to complicated interplay of chemistry and transport caused by net transport of pollution from the northern mid-latitudes and eastern Asia. These values are comparable to TCO values derived from the TOMS/MLS residual. However, the latter shows a uniformly high value in the range of 40–45 DU over most of the midlatitude in the northern hemisphere. Notwithstanding these subtle differences, the model and observations are in general agreement as seen in Table 6. The seasonal differences between model and observations are similar in other months. In general, the differences are pronounced during winter and spring months in both hemispheres. The model values are persistently higher than the observed values by 10–15 DU.

[37] The TOMS/MLS and model differences are corroborated by ozonesonde data as seen in Figure 13. Figure 13 compares the seasonal variations in TCO inferred from the GEOS-CHEM model with TCO derived from TOMS/MLS residual and sonde measurements at two sonde locations, Hilo, Hawaii (20°N, 155°W) and Naha, Japan (26°N, 128°E). At both locations sonde data tend to support lower TCO values in winter months compared to model. During winter, sondes for the same year indicate values 5-1 DU lower than the model, while sondes for the long term record indicate values 5–10 DU lower than the model. We note that TOMS/MLS residual at both Hilo and Naha is lower than sonde by 5–10 DU in winter/spring months. The main point is that differences remain between model and observations in these months.

[38] Figure 14 compares the seasonal variations in ozone in the lower (ground to 500 hPa) and the upper troposphere (500 hPa to tropopause) as inferred from the sonde data at

Table 5. Same as Table 3 but for February 1997 in Figure 12

Latitudes	TOMS/MLS-Model	RMS	r
20N–30N	−15.6	16.5	0.46
10N–20N	−14.0	14.5	0.70
0N–10N	−5.3	6.9	0.72
0S–10S	0.9	3.3	0.89
10S–20S	0.5	3.3	0.81
20S–30S	0.7	3.6	0.55

Table 6. Same as Table 3 but for July 1997 in Figure 12

Latitudes	TOMS/MLS-Model	RMS	r
20N–30N	3.5	7.1	0.30
10N–20N	3.6	5.7	0.73
0N–10N	4.2	5.5	0.85
0S–10S	−1.8	4.0	0.86
10S–20S	−7.4	8.0	0.85
20S–30S	−5.0	8.5	0.25

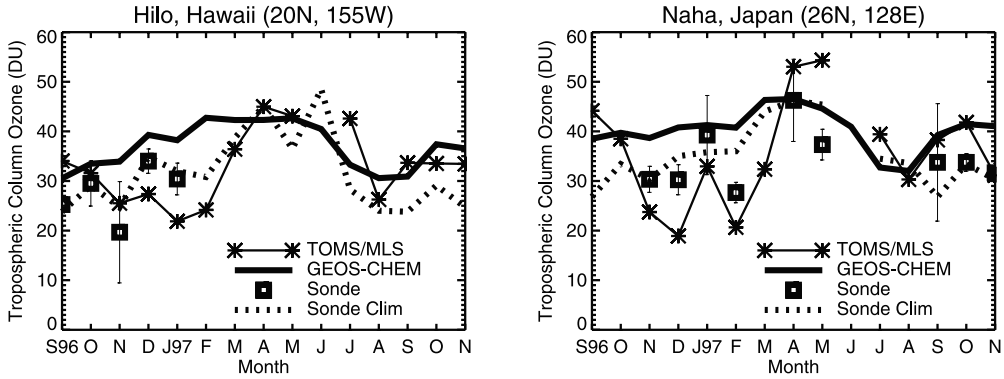

Figure 13. Left: TOMS/MLS (stars), GEOS-CHEM model (dotted), and ozonesonde (boxes with 1σ error bars) monthly mean TCO time series for September 1996–November 1997 at Hilo Hawaii (20°N, 155 °W). Right: Same as left frame but for Naha, Japan (26°N, 128°E). Shown in these figures is also the TCO climatology based on sonde data (dotted lines).

Hilo and Naha with the GEOS-CHEM model. In both the upper and the lower troposphere the model values tend to be higher by 5–10 DU compared to sonde values during winter. *Chan et al.* [1998] attributed the wintertime ozone minimum observed by sondes at Hong Kong (22°N, 114°E) to a tropical influence. *Liu et al.* [2002] reproduced in the GEOS-CHEM model the seasonal minimum and high variability in the upper troposphere observed by ozonesondes throughout the Pacific Rim. The high variability reflects alternating intrusions of stratospheric air, and of tropical air to the region. Some of the model bias shown here may reflect sampling since modeled ozone values are averaged over the entire month, while the ozonesondes and TOMS/MLS data are comprised of a few observations per month. However comparison of ozonesondes with model values for the same day by *Liu et al.* [2002] shows an occasional model bias of greater than 10 ppbv with respect to ozonesondes in the upper troposphere at Hilo and Naha. The long-term ozone-

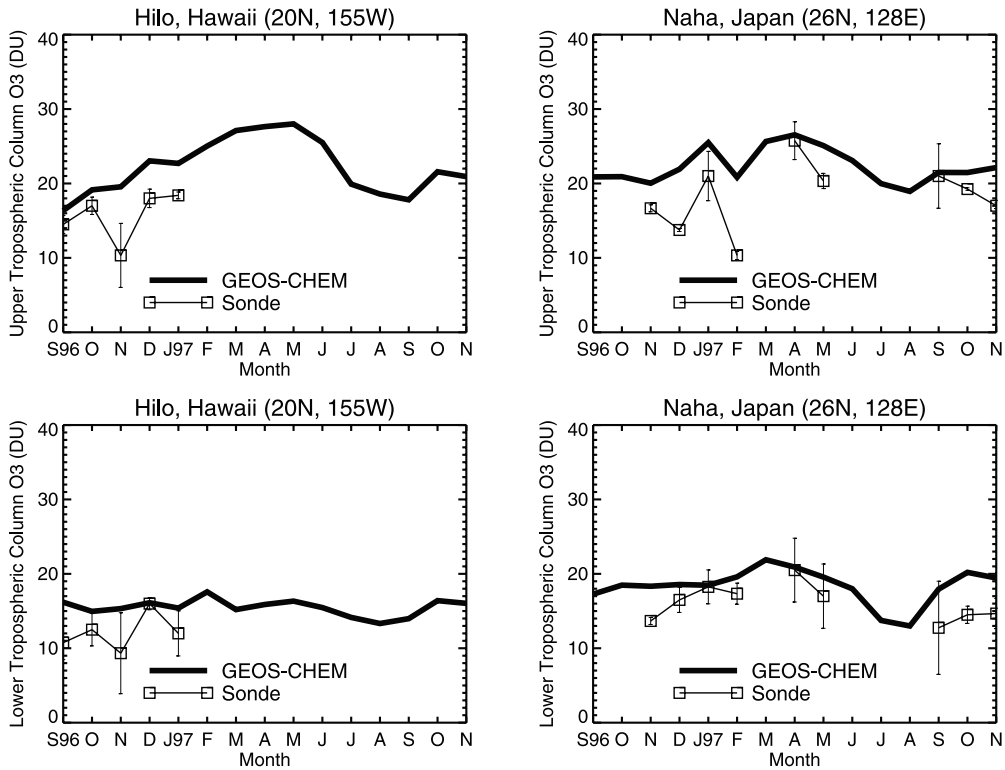

Figure 14. Top left: GEOS-CHEM model (stars), and ozonesonde (boxes with 1σ error bars) monthly mean above-500 hPa (i.e., upper troposphere) column ozone time series for September 1996-November 1997 at Hilo Hawaii (20°N, 155°W). Top right: Same as left frame but for Naha, Japan (26°N, 128°E). The bottom frames are same as top two frames in figure except for below-500 hPa (i.e., lower troposphere) column ozone.

sonde record (Figure 13) suggests a similar model bias. Models also have difficulty in reproducing aircraft observations of less than 30 ppbv in the lower troposphere over the northern Tropical Pacific [*Staudt et al.*, 2002].

10. Summary and Conclusions

[39] In this paper, we have derived daily and monthly maps of TCO at tropical and middle latitudes based on the TOR principle, which uses concurrent measurements of total column ozone from the TOMS (version 7) instrument and SCO from the MLS (version 5) instrument on UARS. The key to the success of this method is calibration of the MLS SCO data to be compatible with TOMS measurements. This is achieved by applying CCD derived SCO measurements as a transfer standard. Because the MLS ozone measurements are limited to regions above 100 hPa, TOMS/MLS residual, in principle, is capable of producing global maps of column ozone from ground-to-100 km. Comparison with ozonesonde data suggests that at latitudes greater than 30°, TOMS/MLS residual has a significant contribution from the stratosphere, which increases rapidly towards higher latitude with the increase of tropopause pressure. The stratospheric contribution has a strong seasonal dependence with maximum contribution during spring months when tropopause pressure is higher than 100 hPa. Over most of the regions between 30°S and 30°N the tropopause pressure is close to 100 hPa and the TOMS/MLS residual can be used to generate TCO maps with only a minor adjustment for tropopause pressure.

[40] Our study has shown that the zonal variability in TOMS total column ozone at tropical and subtropical latitudes is mostly of tropospheric origin. The zonal contrast in TCO maximizes near the equator and weakens considerably outside the tropics. The tropical zonal contrast is usually characterized by wave 1 except during the 1997–1998 El Niño when TCO was significantly elevated for several months in 1997 over half the tropical belt encompassing South America, Southern Africa and Indonesia. The seasonal and zonal variability in TCO in the tropics, derived from the TOMS/MLS residual, are consistent with those derived from the CCD method and ozonesonde data both for El Niño and non-El Niño years.

[41] A comparison of TCO derived from the TOMS/MLS residual and GEOS-CHEM model for the 1996–1997 period shows good agreement in the tropics south of the equator consistent with the previous studies [*Chandra et al.*, 2002]. Both the model and observations show similar zonal and seasonal characteristics including the enhancement of TCO in the Indonesian region associated with El Niño in 1997, and the poleward decline of the wave-1 pattern associated with the decline of lightning activity and the large-scale Walker Circulation. The model and observational differences increase with latitude during winter and spring.

[42] The methodology for deriving TCO using TOMS/MLS residual is limited to ±30° in latitudes because the MLS instrument on UARS cannot measure ozone below 100 hPa. This restriction should not apply to future satellite missions. For example, OMI, HIRDLS, and MLS instruments to be launched on the EOS Aura satellite in year 2004 should provide global measurements of column ozone and ozone profiles in the stratosphere down to the tropopause.

[43] **Acknowledgments.** We are thankful to the UARS MLS team for their efforts in providing the MLS ozone data used in this study. We also thank P. K. Bhartia and D. J. Jacob for helpful comments. The GEOS-CHEM model was developed at Harvard University and was funded by the NASA Atmospheric Chemistry Modeling and Analysis Program. Randall V. Martin was supported by a National Defense and Engineering Graduate Fellowship.

References

Bey, I., D. J. Jacob, R. M. Yantosca, J. A. Logan, B. D. Field, A. M. Fiore, Q. Li, H. Y. Liu, L. J. Mickley, and M. G. Schultz, Global modeling of tropospheric chemistry with assimilated meteorology: Model description and evaluation, *J. Geophys. Res.*, *106*, 23,073–23,096, 2001a.

Bey, I., D. J. Jacob, J. A. Logan, and R. M. Yantosca, Asian chemical outflow to the Pacific: Origins, pathways and budgets, *J. Geophys. Res.*, *106*, 23,097–23,114, 2001b.

Brühl, C., et al., Halogen Occultation Experiment ozone channel validation, *J. Geophys. Res.*, *101*, 10,217–10,240, 1996.

Chan, L. Y., H. Y. Liu, K. S. Lam, and T. Wang, Analysis of the seasonal behaviour of tropospheric ozone at Hong Kong, *Atmos. Environ.*, *32*, 159–168, 1998.

Chandra, S., J. R. Ziemke, W. Min, and W. G. Read, Effects of 1997–1998 El Niño on tropospheric ozone and water vapor, *Geophys. Res. Lett.*, *25*, 3867–3870, 1998.

Chandra, S., J. R. Ziemke, P. K. Bhartia, and R. V. Martin, Tropical tropospheric ozone: Implications for dynamics and biomass burning, *J. Geophys., Res.*, *107*(D14), 4188, doi:10.129/2001JD000447, 2002.

Duncan, B. N., R. V. Martin, A. C. Staudt, R. M. Yevich, and J. A. Logan, Interannual and seasonal variability of biomass burning emissions constrained by satellite observations, *J. Geophys. Res.*, *108*(D2), 4100, doi:10.1029/2002JD002378, 2003.

Fiore, A. M., D. J. Jacob, I. Bey, R. M. Yantosca, B. D. Field, and J. G. Wilkinson, Background ozone over the United States in summer: Origin, trend, and contribution to pollution episodes, *J. Geophys. Res.*, *107*(D15), 4275, doi:10.1029/2001JD000982, 2002.

Fishman, J., and A. E. Balok, Calculation of daily tropospheric ozone residuals using TOMS and empirically improved SBUV measurements: Application to an ozone pollution episode over the eastern United States, *J. Geophys. Res.*, *104*, 30,319–30,340, 1999.

Fishman, J., and J. C. Larsen, Distribution of total ozone and stratospheric ozone in the tropics: Implications for the distribution of tropospheric ozone, *J. Geophys. Res.*, *92*, 6627–6634, 1987.

Fishman, J., C. E. Watson, J. C. Larsen, and J. A. Logan, Distribution of tropospheric ozone determined from satellite data, *J. Geophys. Res.*, *95*, 3599–3617, 1990.

Fishman, J., V. G. Brackett, E. V. Browell, and W. B. Grant, Tropospheric ozone derived from TOMS/SBUV measurements during TRACE A, *J. Geophys. Res.*, *101*, 24,069–24,082, 1996.

Froidevaux, L., et al., Validation of UARS Microwave Limb Sounder ozone measurements, *J. Geophys. Res.*, *101*, 10,017–10,060, 1996.

Fujiwara, M., K. Kita, S. Kawakami, T. Ogawa, N. Komala, S. Saraspriya, and A. Suripto, Tropospheric ozone enhancements during the Indonesian forest fire events in 1994 and in 1997 as revealed by ground-based observations, *Geophys. Res. Lett.*, *26*, 2417–2420, 1999.

Guenther, A., A global model of natural volatile organic compound emissions, *J. Geophys. Res.*, *100*, 8873–8892, 1995.

Hudson, R. D., and A. M. Thompson, Tropical tropospheric ozone from total ozone mapping spectrometer by a modified residual method, *J. Geophys. Res.*, *103*, 22,129–22,145, 1998.

Jacob, D. J., Origin of ozone and NO_x in the tropical troposphere: A photochemical analysis of aircraft observations over the South Atlantic basin, *J. Geophys. Res.*, *101*, 24,235–24,250, 1996.

Jacobson, M. Z., and R. P. Turco, SMVGEAR: A sparse-matrix, vectorized Gear code for atmospheric models, *Atmos. Environ.*, *28*, 273–284, 1994.

Jiang, Y. B., and Y. L. Yung, Concentrations of tropospheric ozone from 1979 to 1992 over tropical Pacific South America from TOMS data, *Science*, *272*, 714–716, 1996.

Kim, J. H., and M. J. Newchurch, Climatology and trends of tropospheric ozone over the eastern Pacific Ocean: The influence of biomass burning and tropospheric dynamics, *Geophys. Res. Lett.*, *23*, 3723–3726, 1996.

Kim, J. H., M. J. Newchurch, and K. Han, Distribution of tropical tropospheric ozone determined by the scan-angle method applied to TOMS measurements, *J. Atmos. Sci.*, *58*, 2699–2708, 2001.

Kley, D., P. J. Crutzen, H. G. J. Smit, H. Vomel, S. J. Oltmans, H. Grassi, and V. Ramanathan, Observations of near-zero ozone concentrations over

the convective Pacific: Effects on air chemistry, *Science*, *274*, 230–232, 1996.

Krishnamurti, T. N., H. Fuelberg, M. C. Sinha, D. Oosterhof, E. L. Bensman, and V. B. Kumar, The meteorological environment of the tropospheric ozone maximum over the tropical South Atlantic Ocean, *J. Geophys. Res.*, *98*, 10,621–10,641, 1993.

Krishnamurti, T. N., M. C. Sinha, M. Kanamitsu, D. Oosterhof, H. Fuelberg, R. Chatfield, D. J. Jacob, and J. Logan, Passive tracer transport relevant to the TRACE A experiment, *J. Geophys. Res.*, *101*, 23,889–23,907, 1996.

Li, Q., et al., A tropospheric ozone maximum over the Middle East, *Geophys. Res. Lett.*, *28*, 3235–3238, 2001.

Li, Q., D. J. Jacob, T. D. Fairlie, H. Liu, R. M. Yantosca, and R. V. Martin, Stratospheric versus pollution influences on ozone at Bermuda: Reconciling past analyses, *J. Geophys. Res.*, *107*(D22), 4611, doi:10.1029/2002JD002138, 2002a.

Li, Q., et al., Transatlantic transport of pollution and its effect on surface ozone in Europe and North America, *J. Geophys. Res.*, *107*(D13), 4166, doi:10.1029/2001JD001422, 2002b.

Liu, H., W. L. Chang, S. J. Oltmans, L. Y. Chan, and J. M. Harris, On springtime high ozone events in the lower troposphere from Southeast Asian biomass burning, *Atmos. Environ.*, *33*, 2403–2410, 1999.

Liu, H., D. J. Jacob, L. Y. Chan, S. J. Oltmans, I. Bey, R. M. Yantosca, J. M. Harris, B. N. Duncan, and R. V. Martin, Sources of tropospheric ozone along the Asian Pacific Rim: An analysis of ozonesonde observations, *J. Geophys. Res.*, *107*(D21), 4573, doi:10.1029/2001JD002005, 2002.

Livesey, N. J., et al., The UARS Microwave Limb Sounder version 5 dataset: Theory, characterization and validation, *J. Geophys.*, *108*, doi:10.1029/2002JD002273, in press, 2003.

Logan, J. A., An analysis of ozonesonde data for the troposphere: Recommendations for testing 3-D models and development of a gridded climatology for tropospheric ozone, *J. Geophys. Res.*, *104*, 16,115–16,149, 1999.

Marenco, A., et al., Measurement of ozone and water vapor by Airbus in-service aircraft: The MOZAIC airborne program, An overview, *J. Geophys. Res.*, *103*, 25,631–25,642, 1998.

Martin, R. V., et al., Interpretation of TOMS observations of tropical tropospheric ozone with a global model and in situ observations, *J. Geophys. Res.*, *107*(D18), 4351, doi:10.1029/2001JD001480, 2002.

Martin, R. V., D. J. Jacob, R. M. Yantosca, M. Chin, and P. Ginoux, Global and regional decreases in tropospheric oxidants from photochemical effects of aerosols, *J. Geophys. Res.*, *108*(D3), 4097, doi:10.1029/2002JD002622, 2003.

McLinden, C. A., S. C. Olsen, B. Hannegan, O. Wild, M. J. Prather, and J. Sundet, Stratospheric ozone in 3-D models: A simple chemistry and the cross-tropopause flux, *J. Geophys. Res.*, *105*, 14,653–14,665, 2000.

Moxim, W. J., and H. Levy II, A model analysis of tropical South Atlantic Ocean tropospheric ozone maximum: The interaction of transport and chemistry, *J. Geophys. Res.*, *105*, 17,393–17,415, 2000.

Newchurch, M. J., D. Sun, and J. H. Kim, Zonal wave-1 structure in TOMS tropical stratospheric ozone, *Geophys. Res. Lett.*, *28*, 3151–3154, 2001.

Pickering, K. E., et al., Convective transport of biomass burning emissions over Brazil during Trace A, *J. Geophys. Res.*, *101*, 23,993–24,012, 1996.

Price, C., and D. Rind, A simple lightning parameterization for calculating global lightning distributions, *J. Geophys. Res.*, *97*, 9919–9933, 1992.

Reber, C. A., The Upper Atmosphere Research Satellite (UARS), *Geophys. Res. Lett.*, *20*, 1215–1218, 1993.

Schubert, S. D., R. B. Rood, and J. Pfaendtner, An assimilated data set for Earth Science applications, *Bull. Am. Meteorol. Soc.*, *74*, 2331–2342, 1993.

Shiotani, M., and F. Hasebe, Stratospheric ozone variations in the equatorial region as seen in stratospheric aerosol and gas experiment data, *J. Geophys. Res.*, *99*, 14,575–14,584, 1994.

Staudt, A. C., D. J. Jacob, J. A. Logan, D. Bachiochi, T. N. Krishnamurti, and N. Poisson, Global chemical model analysis of biomass burning and lightning influences over the South Pacific in austral spring, *J. Geophys. Res.*, *107*(D14), 4200, doi:10.1029/2000JD000296, 2002.

Sudo, K., and M. Takahashi, Simulation of tropospheric ozone changes during 1997–1998 El Nino: Meteorological impact on tropospheric photochemistry, *Geophys. Res. Lett.*, *28*, 4091–4094, 2001.

Sudo, K., M. Takahashi, J.-I. Kurokawa, and H. Akimoto, CHASER: A global chemical model of the troposphere: 1, Model description, *J. Geophys. Res.*, *107*(D17), 4339, doi:10.1029/2001JD001113, 2002.

Thompson, A. M., and R. D. Hudson, Tropical tropospheric ozone (TTO) maps from Nimbus 7 and Earth Probe TOMS by the modified-residual method: Evaluation with sondes, ENSO signals, and trends from Atlantic regional time series, *J. Geophys. Res.*, *104*, 26,961–26,975, 1999.

Thompson, A. M., K. E. Pickering, D. P. Menamara, M. R. Schoeberl, R. D. Hudson, J. H. Kim, E. V. Browell, V. W. J. H. Kirchoff, and D. Nganga, Where did tropospheric ozone over southern Africa and the tropical Atlantic come from in October 1992?: Insights from TOMS, GTE TRACE A, and SAFARI 1992, *J. Geophys. Res.*, *101*, 24,251–24,278, 1996.

Thompson, A. M., J. C. Witte, R. D. Hudson, H. Guo, J. R. Herman, and M. Fujiwara, Tropical tropospheric ozone and biomass burning, *Science*, *291*, 2128–2132, 2001.

Thompson, A. M., et al., Southern Hemisphere Additional Ozonesondes (SHADOZ) 1998–2000 tropical ozone climatology: 1. Comparisons with Total Ozone Mapping Spectrometer (TOMS) and ground-based measurements, *J. Geophys. Res.*, *108*(D2), 8238, doi:10.1029/2001JD000967, 2003.

Torres, O., and P. K. Bhartia, Impact of tropospheric aerosol absorption on ozone retrieval from backscattered ultraviolet measurements, *J. Geophys. Res.*, *104*, 21,569–21,577, 1999.

Wang, Y., D. J. Jacob, and J. A. Logan, Global simulation of tropospheric O_3 - NO_x - hydrocarbon chemistry: 1, Model formulation, *J. Geophys. Res.*, *103*, 10,713–10,726, 1998.

Wild, O., X. Zhu, and M. J. Prather, Fast-J: Accurate simulation of in- and below-cloud photolysis in tropospheric chemistry models, *J. Atmos. Chem.*, *37*, 245–282, 2000.

Yienger, J. J., and H. Levy, Empirical model of global soil-biogenic NO_x emissions, *J. Geophys. Res.*, *100*, 11,447–11,464, 1995.

Ziemke, J. R., and S. Chandra, Seasonal and interannual variabilities in tropical tropospheric ozone, *J. Geophys. Res.*, *104*, 21,425–21,442, 1999.

Ziemke, J. R., S. Chandra, A. M. Thompson, and D. P. McNamara, Zonal asymmetries in southern hemisphere column ozone: Implications of biomass burning, *J. Geophys. Res.*, *101*, 14,421–14,427, 1996.

Ziemke, J. R., S. Chandra, and P. K. Bhartia, Two new methods for deriving tropospehric column ozone from TOMS measurements: Assimilated UARS MLS/HALOE and convective-cloud differential techniques, *J. Geophys. Res.*, *103*, 22,115–22,127, 1998.

Ziemke, J. R., S. Chandra, and P. K. Bhartia, "Cloud slicing": A new technique to derive upper tropospheric ozone from satellite measurements, *J. Geophys. Res.*, *106*, 9853–9867, 2001.

S. Chandra and J. R. Ziemke, NASA Goddard Space Flight Center, Code 916, Greenbelt, MD 20771, USA. (chandra@chapman.gsfc.nasa.gov; ziemke@jwocky.gsfc.nasa.gov)

R. V. Martin, Harvard-Smithsonian Center for Astrophysics, Division of Engineering and Applied Sciences, Harvard University, Cambridge, MA 02138, USA. (rvmartin@fas.harvard.edu)